Molecular Therapy
Original Article

# ARI0003: Co-transduced CD19/BCMA dual-targeting CAR-T cells for the treatment of non-Hodgkin lymphoma

Mireia Bachiller,[1,11] Nina Barceló-Genestar,[1,11] Alba Rodriguez-Garcia,[1] Leticia Alserawan,[2] Cèlia Dobaño-López,[1,3] Marta Giménez-Alejandre,[1] Joan Castellsagué,[1] Salut Colell,[1] Marc Otero-Mateo,[1] Asier Antoñana-Vildosola,[1] Marta Español-Rego,[1,2] Noelia Ferruz,[4] Mariona Pascal,[1,2,5] Beatriz Martín-Antonio,[1,6] Xavier M. Anguela,[7] Cristina Fillat,[1,8] Eulàlia Olesti,[1,5,9] Gonzalo Calvo,[1,5,9] Manel Juan,[1,2] Julio Delgado,[1,3,5,10] Patricia Pérez-Galán,[1,3] Álvaro Urbano-Ispizua,[1,5,10,12] and Sonia Guedan[1,12]

[1]Fundació de Recerca Clínic Barcelona-Institut d'Investigacions Biomèdiques August Pi Sunyer (FRCB-IDIBAPS), 08036 Barcelona, Spain; [2]Department of Immunology, Hospital Clínic, 08036 Barcelona, Spain; [3]Centro de Investigación Biomédica en Red-Oncología (CIBERONC), 28029 Madrid, Spain; [4]Centre for Genomic Regulation (CRG), Barcelona Institute for Science and Technology, 08003 Barcelona, Spain; [5]University of Barcelona, 08034 Barcelona, Spain; [6]Instituto de Salud Carlos III, 28029 Madrid, Spain; [7]Estuary Biotherapeutics, Philadelphia, PA 19104, USA; [8]Centro de Investigación en Red-Enfermedades Raras (CIBERER), 08036 Barcelona, Spain; [9]Department of Clinical Pharmacology, Hospital Clínic, 08036 Barcelona, Spain; [10]Department of Hematology, Hospital Clínic, 08036 Barcelona, Spain

**CD19 CAR-T therapy has achieved remarkable responses in relapsed/refractory non-Hodgkin lymphoma (NHL). However, challenges persist, with refractory responses or relapses after CAR-T administration linked to CD19 loss or downregulation. Given the co-expression of CD19 and BCMA in NHL, we hypothesized that dual targeting could enhance long-term efficacy. We optimized different dual-targeting approaches, including co-transduction of two lentiviral vectors, bicistronic, tandem, and loop and pool strategies, based on our academic anti-CD19 (ARI0001) and anti-BCMA (ARI0002h) CAR-T cells. Comparison with anti-CD19/CD20 or anti-CD19/CD22 dual targeting was also performed. We demonstrate that anti-CD19/BCMA CAR-T cells can be effectively generated through the co-transduction of two lentiviral vectors after optimization to minimize competition for cellular resources. Co-transduced T cells, called ARI0003, effectively targeted NHL tumor cells with high avidity, outperforming anti-CD19 CAR-T cells and other dual-targeting approaches both *in vitro* and *in vivo*, particularly in low CD19 antigen density models. ARI0003 maintained effectiveness post-CD19 CAR-T treatment in xenograft models and in spheroids from relapsed CART-treated patients. ARI0003 CAR-T cells were effectively manufactured under Good Manufacturing Practice conditions, with a reduced risk of genotoxicity compared to other dual-targeting approaches. A first-in-human phase 1 clinical trial (CARTD-BG-01; this study was registered at ClinicalTrials.gov [NCT06097455]) has been initiated to evaluate the safety and efficacy of ARI0003 in NHL.**

## INTRODUCTION

Chimeric antigen receptor (CAR) T cell therapy targeting CD19 has demonstrated unprecedented clinical responses in patients with B cell lymphoid malignancies refractory to conventional treatments.[1–8] However, around 50% of patients with large B cell lymphoma do not achieve a complete response (CR), and approximately 40%–50% of patients who achieve a CR subsequently relapse.[3,4,9]

CD19 loss has been widely described after CD19 CAR-T cell relapse in B cell acute lymphoblastic leukemia (ALL) and in diffuse large B cell lymphoma (DLBCL).[10–13] Additionally, interpatient variability of CD19 expression together with heterogeneity in CD19 expression at the time of diagnosis seems to hold special relevance in DLBCL relapses.[14] Diminished expression on CD19 correlates with poor clinical outcomes and reduced event-free survival, suggesting that antigen density below a certain threshold prevents CAR-T cell full activation.[15,16]

Significant efforts are under way to develop dual-targeting CAR-T cells to prevent antigen escape in non-Hodgkin lymphoma (NHL).[17] Dual-targeting strategies include (1) co-administration of two monotargeted CAR-T cells (pooled CAR-T cells), (2) co-transduced CAR-T using two viral vectors, (3) bicistronic CAR-T cells encoding two genetic constructs in a single vector, and (4) tandem or loop CAR-T cells encoding a single CAR molecule with two different targeting moieties. Preclinical studies revealed the superior efficacy of dual-targeting strategies, and initial

Received 9 April 2024; accepted 15 November 2024;
https://doi.org/10.1016/j.ymthe.2024.11.028.

[11]These authors contributed equally

[12]These authors contributed equally

**Correspondence:** Sonia Guedan, Fundació de Recerca Clínic Barcelona-Institut d'Investigacions Biomèdiques August Pi Sunyer (FRCB-IDIBAPS), 08036 Barcelona, Spain.
**E-mail:** sguedan@recerca.clinic.cat

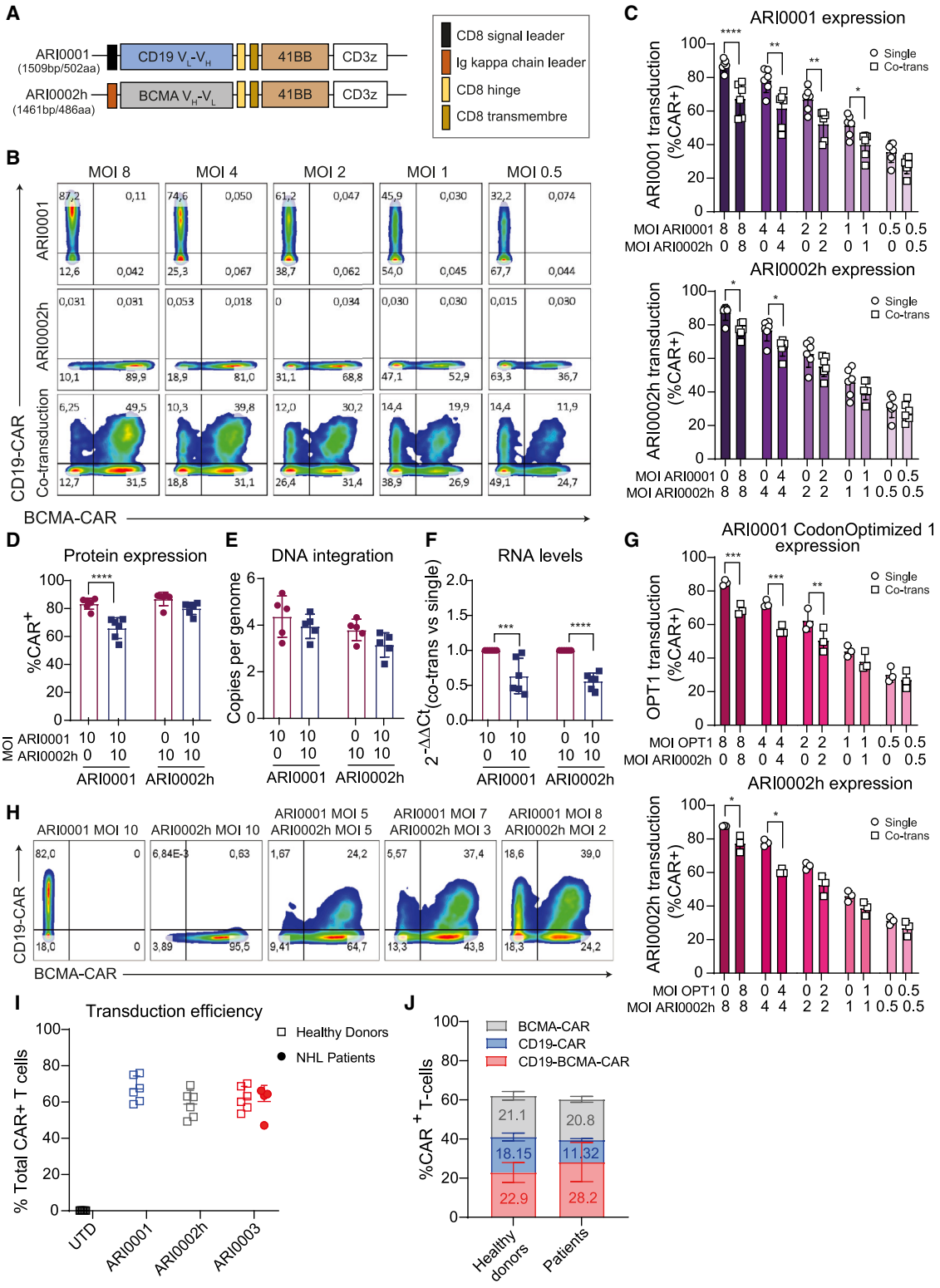


*(legend on next page)*

clinical trials indicated a comparable safety profile between dual- and single-targeting CAR-T cells[18]; in certain instances, antigen loss has been partially mitigated.[19–23] However, the remarkable efficacy of monotargeted CAR-T cells stands out prominently, and there is no solid clinical evidence demonstrating that dual-CAR-T cells yield enhanced therapeutic effects. Unlocking the full potential of dual-CAR-T cells may require the identification of ideal targets, further construct optimization, extensive head-to-head comparisons and a deeper understanding of their mechanism of action.

B cell maturation antigen (BCMA) is expressed during B lymphoid maturation, and its expression is restricted to mature plasma cells, some mature forms of B lymphocytes, and neoplastic plasma cells. Because of this restricted expression, it has emerged as a therapeutic target for multiple myeloma and more recently as a potential target for B cell lymphoma.[24,25] CAR-T cells targeting BCMA have induced sustained responses in patients with relapsed or refractory multiple myeloma with low toxicity.[26–28] However, the potential of BCMA as a therapeutic target for B cell lymphomas has not been clinically evaluated.

In this study, we generated a panel of dual-targeting CD19/BCMA CAR-T cells based on our academic CAR-T cells targeting CD19 (varnimcabtagene autoleucel or ARI0001) and BCMA (cesnicabtagene autoleucel or ARI0002h).[29,30] Both ARI0001 and ARI0002h have been tested in clinical studies for the treatment of B cell leukemias and lymphomas[31–33] and multiple myeloma,[26] respectively, demonstrating safety and efficacy results comparable to those of commercially available products. Here, we present an optimized strategy to generate dual-CAR-T cells containing balanced populations of each CAR by the co-transduction of two lentiviral vectors (LVs), including validation under Good Manufacturing Practices (GMP) conditions. Using various preclinical models, including *in vivo* models of low CD19 densities and NHL patient-derived spheroids, we show that CAR-T cells generated by co-transduction, called ARI0003, demonstrate enhanced efficacy, safety, and feasibility compared to other dual-targeting strategies. Based on these results, we initiated a phase 1 clinical trial in patients with relapsed/refractory NHL (CARTD-BG-01; this study was registered at ClinicalTrials.gov [NCT06097455]).

## RESULTS

### Co-transduction of two LVs enables dual-CAR expression despite competition for cellular resources

To assess the potential synergistic activity of co-targeting CD19 and BCMA, we co-transduced T cells with two LVs. As cellular resources are limited,[34] we hypothesized that the co-expression of two CARs within a T cell may compete for the use of cellular machinery. To test this hypothesis, we transduced T cells with two LVs: ARI0001 (anti-CD19 CAR) and ARI0002h (anti-BCMA CAR) (Figure 1A). These two LVs were used either individually or at different ratios to each other, along a range of increasing MOIs to represent different levels of saturation of the cellular machinery (Figures 1B and 1C). As expected, the expression of ARI0001 and ARI0002h following single lentiviral transductions increased proportionally with MOI (Figure 1B). Surprisingly, co-transduction led to reduced ARI0001 expression, favoring ARI0002h at all MOIs (Figure 1B). This imbalance intensified at higher MOIs, indicating that the simultaneous expression of multiple transgenes under high transgene load can lead to a stronger rivalry for essential cellular machinery involved in gene expression, ultimately resulting in impaired protein production (Figure 1C). Although the percentage of ARI0002h$^+$ cells also decreased following the co-transduction of two LVs at the highest MOIs, this decrease appeared to be less pronounced than in the case of ARI0001. Notably, both CARs showed lower mean fluorescence intensity (MFI) when co-transduced than when transduced individually (Figure S1A). Interestingly, ARI0001 also displayed a reduced protein expression when co-transduced with other CARs (i.e., HER2-28Z or mesothelin-BBZ), suggesting that this loss is not specific for co-transduction with ARI0002h (Figures S1B and S1C). The fact that all constructs were of similar size and that combinations of ARI0001 with CAR constructs containing the same or different signal peptides (CD8a vs. immunoglobulin [Ig] kappa chain) or co-stimulatory domains (4-1BB vs. CD28) were included ruled out these factors as responsible for the reduction in ARI0001 expression.

To gain a better understanding of which intracellular resources may become rate limiting for optimal transgene expression, we quantified vector DNA and mRNA expression at a high MOI for both LVs. Despite the observed differences in CAR protein expression (Figure 1D), vector copy numbers (VCNs) were not different between single- or co-transduction conditions for either LV (Figure 1E).

**Figure 1. Generation of dual-targeting CAR-T cells by co-transduction of lentiviral vectors**

(A) Schematic representation of CAR constructs. (B) Representative flow cytometry plots of CAR staining on the T cell membrane in single transduction for ARI0001 (top), for ARI0002h (center), and in co-transduction (bottom) at the indicated MOIs. (C) Quantification of CAR expression shown in (B). Bar graphs depict mean percentage of transduction in single or co-transduction ±SD ($n = 6$ healthy donors). Two-way ANOVA tests. *$p < 0.05$; **$p < 0.005$; ***$p < 0.0005$; ****$p < 0.0001$. (D–F) T cells after single or co-transduction with high MOIs (MOI = 10) were studied at protein (D), DNA (E), and RNA (F) levels. Bar graphs depict mean ± SD. Each dot represents a healthy donor ($n = 5$). (D) Percentage of CAR expression on the T cell membrane analyzed by flow cytometry. (E) Integrated DNA LV copies per genome determined by qPCR ($n = 6$). (F) CAR mRNA levels in co-transduced and single-transduced CAR-T cells determined by real-time PCR ($n = 6$). (G) Quantification of CAR expression for the ARI0001 CAR codon optimized version 1 (top) and for the ARI0002h CAR (bottom) after single- and co-transduction ($n = 3$). Two-way ANOVA tests. *$p < 0.05$; **$p < 0.005$; ***$p < 0.0005$; ****$p < 0.0001$. (H) Representative flow cytometry plots of CAR staining on the T cell. An MOI of 10 was used for single transductions, while three combinations of MOIs were used for CAR co-transduction. Representative of two experiments using different healthy donors. (I) Percentage of CAR$^+$-T cells after transduction with a single LV or after co-transduction (ARI0003). Each dot represents a donor ($n = 6$ for healthy donors and $n = 4$ for NHL patients). (J) CAR distribution within the CAR$^+$ population of ARI0003. Mean ± SD from $n = 6$ healthy donors and $n = 4$ NHL patients.

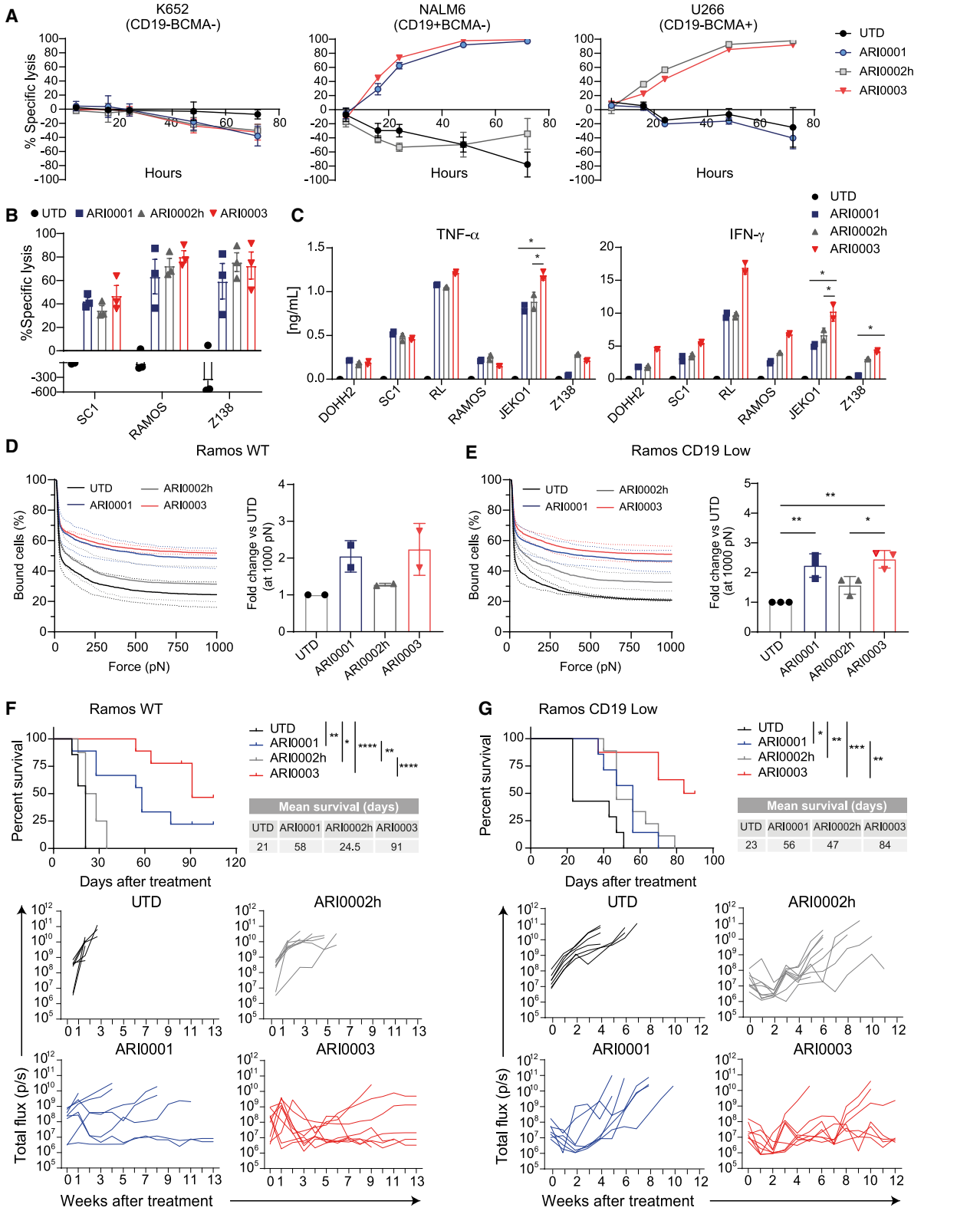


*(legend on next page)*

Sequential transduction (ARI0001 at 16 h post-activation and ARI0002h at 24 h) failed to alleviate the decrease in ARI0001 expression after co-transduction (Figure S1D). Moreover, CAR mRNA levels decreased after co-transduction for both LVs (Figure 1F), suggesting that while the transcriptional machinery is sensitive to transgene burden, this cannot fully explain the preferential expression of the BCMA CAR over the CD19 CAR in overloaded cellular conditions.

As codon optimization has been postulated as a critical determinant for increasing mRNA stability and protein expression,[35] we tested three optimized versions of ARI0001 CAR in co-transduction with ARI0002h (Figures 1G and S2A). While the Codon Adaptation Index, which quantifies the compatibility of codon usage with the host's preferred codon frequency, was similar for all four ARI0001 sequences and deemed favorable for expression in human cells, the three optimized sequences displayed increased percentages of GC content, particularly that of the third base position GC3, a feature associated with high mRNA stability and translational efficiency (Figure S2B).[36] Optimized versions displayed a more stable distribution of codon usage frequency along the length of the sequence, suggesting harmonized gene expression (Figure S2C). The three optimized sequences demonstrated heightened MFIs compared to the parental ARI0001 following single lentiviral transduction, even though the CAR percentage remained uniform across all constructs (Figure S2D). However, screening of codon-optimized CAR versions did not lessen the decreased ARI0001 CAR expression after co-transduction (Figures 1G and S2A).

Given that codon optimization failed to address the imbalance in CAR expression (Figure S2) and considering the excellent clinical results of ARI0001 in treating lymphoma patients,[33] we aimed to address the imbalance without altering ARI0001. For that, we used different ratios of ARI0001:ARI0002h MOIs (5:5, 7:3, and 8:2) that favored an increase in the amount of ARI0001 vector and a decrease in ARI0002h (Figure 1H). Using MOI = 8 for ARI0001 and MOI = 2 for ARI0002h, we obtained a dual-CAR-T cell product with balanced populations that were homogeneous among different healthy donors (Figures 1I and 1J). On the basis of this, we defined the anti-CD19/BCMA dual-CAR-T cell product, called ARI0003, as the co-transduction of four times fewer ARI0002h than ARI0001. ARI0003 exhibited a 60% mean transduction efficiency across healthy donors and NHL patients, akin to single CARs (Figure 1I). ARI0003 comprises three $CAR^+$ populations, with dual-CAR expression ranging between 15% and 30% for both healthy donors and NHL patients (Figure 1J).

### ARI0003 is effective against NHL models

We first addressed whether ARI0003 CAR-T cells were at least as effective as monospecific CAR-T cells when just one antigen was present. ARI0003 matched the potency of monospecific CAR-T cells targeting either an ALL-derived cell line (NALM6, $CD19^+$) or a multiple myeloma-derived cell line (U266, $BCMA^+$) (Figures 2A and S3). Then, we performed functional analysis of ARI0003 in short-term co-cultures with a panel of NHL cell lines. The expression levels of BCMA in NHL cell lines were analyzed in comparison to CD19, CD20, and CD22, three commonly targeted antigens in CAR-T cell therapy for hematologic malignancies. In general, NHL cell lines presented high densities of CD19 and CD20, while BCMA expression was lower, following a pattern similar to that of CD22 (Figure S4). Despite low BCMA densities, ARI0002h cells were able to exhibit robust activation and eliminate NHL tumor cells similar to ARI0001 (Figure 2B). Cytotoxicity and cytokine production were similar across dual- and mono-targeting CAR-T cell groups, except for JEKO1 and Z138 cell lines, in which significant increases in interferon-$\gamma$ (IFN-$\gamma$) and tumor necrosis factor $\alpha$ (TNF-$\alpha$) secretion were observed with ARI0003 (Figures 2B and 2C). We next aimed to determine whether dual targeting of CD19 and BCMA enhanced CAR-T cell-binding strength to target cells. To assess this, we performed avidity assays on a Burkitt lymphoma (BL) cell line expressing low endogenous BCMA densities and either high CD19 endogenous densities (Ramos wild type [WT]) or genetically modified to express low CD19 densities (Ramos CD19 Low), a characteristic associated with treatment failure (Figure S4). Both ARI0001 and ARI0003 showed increased avidity compared to ARI0002h in both target cell types, with ARI0003 displaying a trend toward higher avidity than ARI0001, particularly in the CD19 low setting, although differences were not statistically significant (Figures 2D and 2E).

As disease burden negatively correlates with CAR-T therapy outcomes,[37] we challenged CAR-T cells with high disease burden Ramos

**Figure 2. ARI0003 cytokine production, cytotoxicity, and *in vivo* antitumor effects**

(A) Control T and CAR-T cells were cultured with the indicated target cells at an E:T ratio of 1:3. A Bioluminescence imaging (BLI)-based killing assay was used to evaluate the lysis of the indicated tumor cell lines over time. The mean ± SD of triplicates from a healthy donor is shown. Representative of two different experiments with two healthy donors ($n = 2$). (B and C) Control T and CAR-T cells were co-cultured with the indicated target cells at an E:T ratio of 1:1 in (B) and 3:1 in (C). Bar graphs depict mean ± SD. Each point represents a healthy donor ($n = 3$). (B) Specific tumor lysis was calculated relative to target cells without treatment using a 16-h luciferase-based killing assay. (C) Supernatants were collected 24 h after co-culture, and the release of TNF-$\alpha$ and IFN-$\gamma$ was analyzed by ELISA. (D and E) The strength of interaction between single- and dual-targeting T cells and Ramos WT (D) or Ramos CD19 Low (E) target cells was measured. The percentage of total CAR-T cells remaining bound to target cells as the acoustic force ramp is applied from 0 to 1,000 pN is shown (right). The fold change of bound CAR-T cells at 1,000 pN as compared to UTD is shown (left). Data are presented as means ± SEMs from two (Ramos WT) or three (Ramos CD19 Low) healthy donors in technical triplicate (n = 2–3). $p$ values were calculated using a one-way ANOVA test. *$p < 0.05$; **$p < 0.01$. (F) "Advanced" Burkitt lymphoma model. NSG mice were i.v. injected with Ramos-GFP-luciferase cells. After 14 days, mice were randomized and treated with $3 \times 10^6$ T cells, including UTD control T cells ($n = 4$), ARI0001 ($n = 6$), ARI0002h ($n = 6$), or ARI0003 ($n = 6$). The Kaplan-Meier survival curves of treated mice are plotted, and mean survival (days) calculated. (G) "Advanced" Burkitt lymphoma model with low CD19 densities. NSG mice were i.v. injected with Ramos-GFP-luciferase-CD19 Low cells. After 14 days, mice were randomized and treated with $2 \times 10^6$ control T cells ($n = 7$) or $CAR^+$-T cells, including ARI0001 ($n = 7$), ARI0002h ($n = 9$), or ARI0003 ($n = 8$). The Kaplan-Meier survival curves of treated mice are plotted and mean survival (days) calculated. Log rank (Mantel-Cox) test. *$p < 0.05$; **$p < 0.005$; ***$p < 0.0005$; ****$p < 0.0001$.

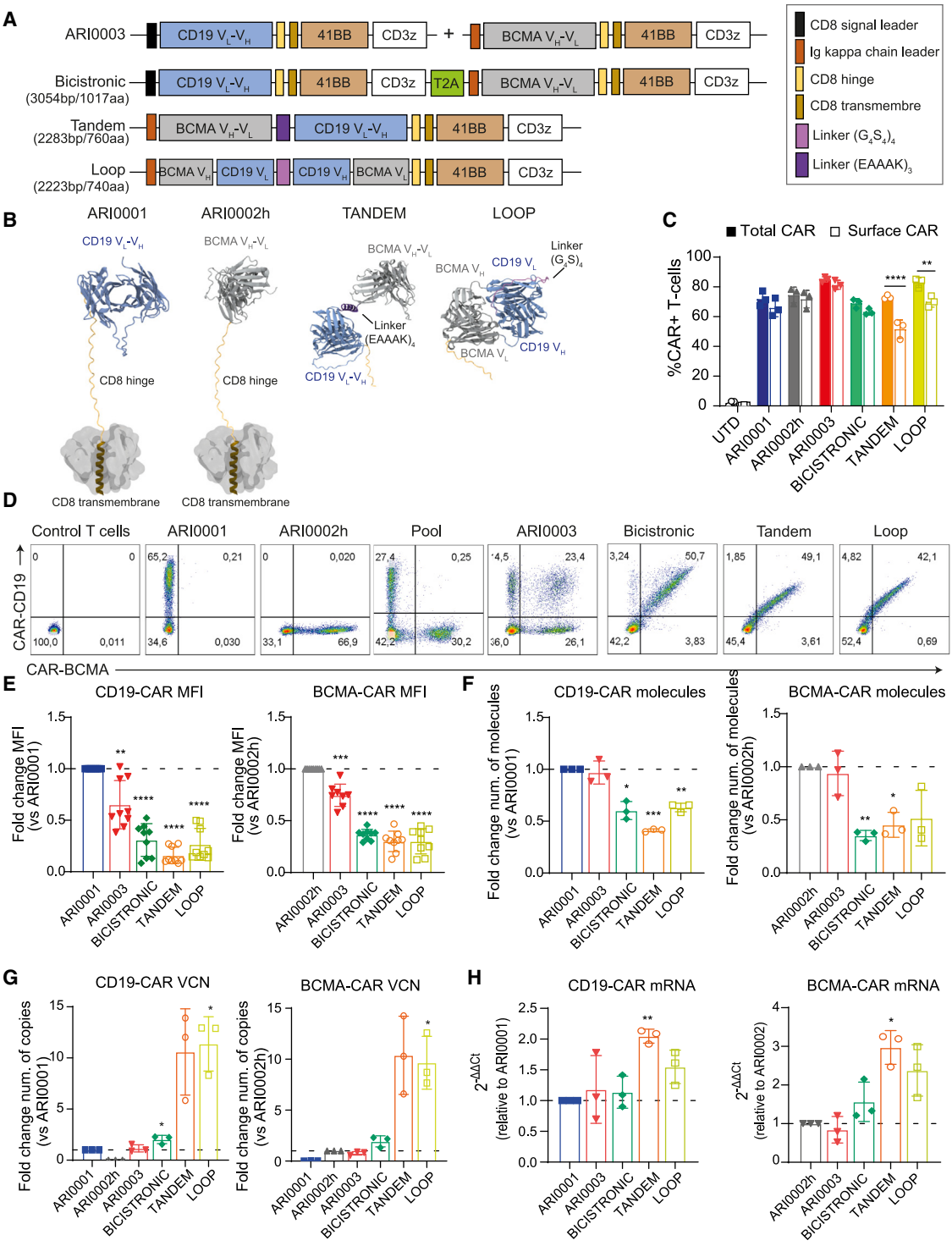


**Figure 3. Generation and expression characterization of different CD19-BCMA dual-targeting strategies**

(A) Schematic representation of CAR constructs. (B) Structural models of CAR constructs were generated using AlphaFold3, based on the input sequences of their extracellular domains (CD8α hinge and scFv). The BCMA-targeting regions are depicted in gray, the CD19-targeting regions in blue, the linkers connecting both regions are shown in purple, and the CD8 hinge in yellow. (C and D) CAR expression on the T cell membrane was analyzed by flow cytometry. (C) Levels of extracellular CAR and total CAR from single and dual-targeting strategies are shown. Bar graphs show the mean ± SD (*n* = 3 healthy donors). Total CAR was assessed using intracellular staining.

*(legend continued on next page)*

WT or Ramos CD19 Low xenograft models. *In vivo* analysis revealed extended mice survival for all CAR-T cell therapies compared to control T cells in the CD19 high-expressing setting. ARI0001 and ARI0003 significantly outperformed ARI0002h, with ARI0003 showing prolonged mice survival (Figure 2F). In the model with low CD19 densities, dual-targeting treatments significantly improved mice survival compared to the control T cells. ARI0003 significantly outperformed ARI0001 (Figure 2G), suggesting that dual targeting might be especially beneficial in patients with malignant B cells that express low antigen densities.

### Generation and expression characterization of diverse modalities of dual-CAR-T cells

After confirming the benefits of co-targeting CD19 and BCMA for NHL, we developed alternative dual strategies to determine the best candidate for clinical translation (Figure 3A). We first focused on developing a series of tandem (four configurations) and loop (two configurations) CARs by combining two single-chain variable fragments (scFvs) and a single intracellular module using different linkers (Figures 3A and S5). To explore potential structural problems in these construct designs, we first performed structural prediction analysis. These studies revealed that while the predicted binding interfaces for CD19 and BCMA remained accessible in all configurations, the positions of the scFvs remain available for interaction between themselves in Tandems1–3, thus competing with their respective binders (Figure S5E). In contrast, the higher rigidity of the Tandem4 and Loop structures, locked in their conformations via their linker and lack of flexible moieties, respectively, prevented this interaction (Figure 3B). To select the most promising candidates and confirm the structural predictions at a functional level, we next assessed CAR expression and specific lysis against cells expressing only one antigen, to ensure productive signaling from both antigen-binding domains of the dual receptor. All constructs were detected on the T cell surface except for Loop1, which was excluded in further experiments (Figures S5B and S5C). While all the constructs except for Tandem3 killed BCMA-expressing target cells as efficiently as ARI0002h, only Tandem4 and Loop2 killed CD19-expressing target cells similar to ARI0001 (Figure S5E). These findings align with our structural predictions and with previous studies indicating that rigid linkers outperform flexible ones.[18,20] The selected candidates, Tandem4 and Loop2, are from this point on referred to as tandem and loop, respectively.

We next compared different dual-targeting strategies, including pooled CAR-T cells, co-transduction, bicistronic, tandem, and loop receptors. Although all CARs were expressed on the surface of T cells at high frequencies (Figures 3C and 3D), the dual-targeting approaches showed lower receptor densities compared to single CAR-T cells, with the co-transduction product, ARI0003, exhibiting the less-pronounced differences (Figures 3E, 3F, and S6C). In addition, we compared surface CAR expression versus total CAR (intracellular staining). Single CAR-T cells, as well as co-transduced (ARI0003) and bicistronic dual-CAR-T cells, showed similar frequencies of surface and total $CAR^+$-T cells. In contrast, tandem and loop constructs had reduced surface $CAR^+$ frequencies, indicating that a portion of the CAR molecules remains intracellular, possibly due to reduced stability on the cell surface (Figure 3C).

To investigate potential issues at the DNA or RNA level, we measured integrated DNA VCNs and CAR mRNA levels. Interestingly, the tandem and loop CAR-T constructs exhibited higher lentiviral DNA integration per genome compared to single CARs or co-transduction, suggesting that they require more vector copies per genome to achieve the same percentage of $CAR^+$-T cells, raising potential safety concerns (Figures 3G, S6A, and S6B). Of note, the bicistronic construct also showed increased VCN, but the differences were smaller.

mRNA levels correlated with VCN across all constructs, indicating that higher integration boosts transcription. However, in the tandem and loop constructs, despite a 10-fold increase in DNA integration, mRNA levels were only elevated 2-fold (Figure 3H). In the same line, despite a 2-fold increase in VCN in the bicistronic construct, mRNA levels were similar to those in ARI0003 or single CARs. These findings suggest that transcriptional limitations, although present in larger constructs, do not fully account for the lower CAR expression. In the case of the bicistronic construct, the observation that similar RNA levels produce fewer protein molecules suggests other potential issues, likely related to inefficient T2A peptide processing.

### ARI0003 exhibits superior antitumor efficacy compared to alternative dual-targeting strategies in NHL models

To validate the targeting efficacy of dual-CAR-T cells upon antigen encounter, we established a K562 model with target cells expressing either one or both antigens at similar densities (Figure 4A). In the presence of only one antigen, dual-targeting CAR-T cells showed similar specific lysis compared to single-targeting CARs. When the targeted cells contained both antigens, the specific lysis by dual groups was either equal or slightly better than that achieved by monospecific CARs (Figure 4B).

We next performed binding avidity experiments to assess the strength of cell-cell interactions across the different dual-CAR approaches. In Ramos WT, loop CAR-T cells exhibited the highest avidity, while the

Statistical analysis was performed using a two-way ANOVA. $^{**}p < 0.005$; $^{****}p < 0.0001$. (D) Flow cytometry plots from a representative healthy donor showing CD19-CAR and/or BCMA-CAR expression on the surface of T cells. (E and F) The CAR mean fluorescence intensity (E) and (F) the number of CAR molecules of dual-targeting strategies compared to ARI0001 (left) or ARI0002h (right) are shown (n = 3–6 healthy donors). The fold decrease in MFI and CAR molecule count relative to single-CAR constructs is calculated and analyzed using a one-sample t test. $^{**}p < 0.005$; $^{***}p < 0.0005$; $^{****}p < 0.0001$. (G and H) Single and dual-targeting strategies were studied at both the DNA (G) and RNA (H) levels. (G) The number of lentiviral DNA copies integrated per genome for CD19 CARs (left) and BCMA CARs (right) compared to ARI0001 or ARI0002h was assessed using qPCR ($n = 3$ healthy donors) and analyzed using the one-sample t test. ANOVA test. $^{*}p < 0.05$. (H) CAR RNA levels in the dual-targeting strategies compared to ARI0001 (left) or ARI0002h (right) were measured by real-time PCR ($n = 3$ healthy donors) and analyzed using a one-sample t test. $^{*}p < 0.05$; $^{**}p < 0.005$.

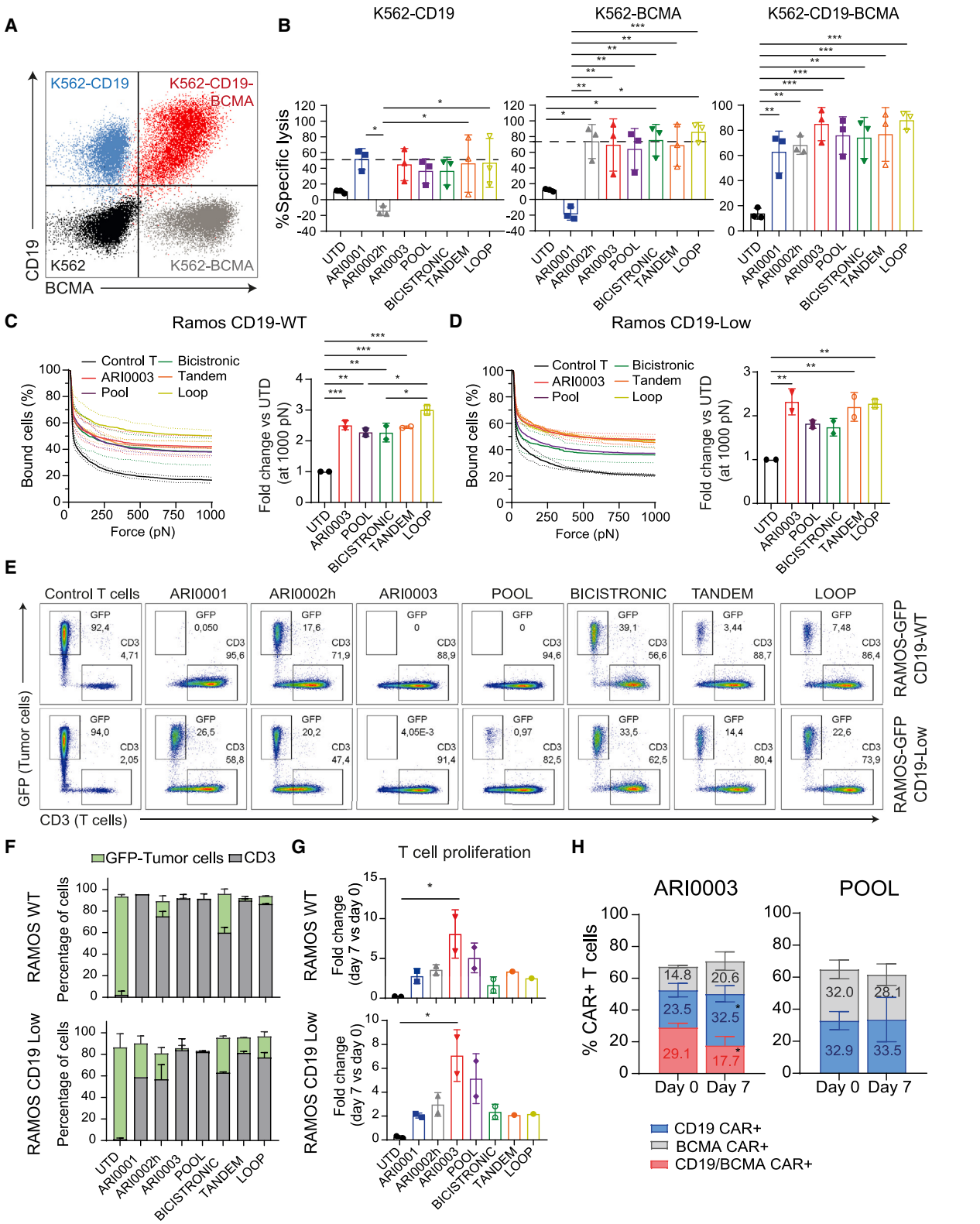


*(legend on next page)*

other groups showed comparable results (Figure 4C). However, under CD19 low conditions (Ramos CD19 Low), the advantage of the loop CAR construct was lost, with its avidity resembling that of ARI0003 and tandem CAR-T cells. Notably, the bicistronic construct demonstrated reduced avidity, similar to that of the pool group (Figure 4D).

We next performed CAR-T cell proliferation and long-term cytotoxicity. ARI0001 effectively eliminated all Ramos WT cells, but its cytotoxicity was compromised at low CD19 antigen densities. ARI0002h, bicistronic, tandem, and loop CAR-T cells failed to enhance ARI0001 activity or sustain tumor elimination, despite the high avidity shown by tandem and loop constructs (Figures 4E and 4F). In contrast, co-transduction and pool CAR-T cells demonstrated consistent tumor elimination, irrespective of CD19 levels (Figures 4E and 4F), along with improved T cell proliferation (Figure 4G). Of note, ARI0003 was the only group that demonstrated significantly increased T cell proliferation after long-term co-culture with both Ramos WT and Ramos CD19 Low. Based on these results and their impaired CAR expression (Figure 3), tandem and loop were excluded from further experiments.

To evaluate the role of the double-positive CAR population within ARI0003, we analyzed the distribution of $CAR^+$ populations for ARI0003 and pooled CAR-T cells at the end of the 7-day co-culture with Ramos WT cells. While in the pool strategy, distribution of CD19- and BCMA-targeting CAR populations remained unaltered as compared to the initial product; in the ARI0003 group we could observe an enrichment of the monospecific CAR populations (more pronounced for CD19 $CAR^+$-T cells) and a concomitant reduction in the double-positive population (Figure 4H). These results suggest that while that dual-targeting T cells could offer an initial functional advantage, they might eventually become exhausted and diminish over time.

Next, we moved to the *in vivo* setting and performed a dose-limiting test treating NOD-SCID gamma (NSG) mice with BL (Ramos WT) with low doses of effector cells (Figures 5A and 5B). Treatment with ARI0001, pool, and bicistronic CAR-T cells resulted in comparable animal mean survival (Figure 5B). In these groups, 25% of the animals treated remained disease-free until the end of the experiment, indicating a modest but significant response. ARI0003 displayed superior efficacy compared to the other tested approaches, although differences in this setting of high CD19 expression did not reach statistical significance. The mean survival was not reached for ARI0003, with 60% of the animals being disease-free at the end of the experiment (Figures 5A and 5B).

To further characterize ARI0003 activity, a novel preclinical model based on patient-derived lymphoma spheroids (PDLS) was generated from primary tumor samples from four different NHL patients and used for *in vitro* studies (Tables S1 and S2). Variable percentages and densities of CD19 and BCMA antigen expression were observed (Figures 5C and S7). Images of representative PDLS from a follicular lymphoma (FL) patient showed T cell infiltration and loss of PDLS sphericity after CAR-T cell treatment (Figure 5D). In all four cases, specific lysis and cytokine release were either similar or slightly better for ARI0003 when compared to ARI0001 (Figures 5E, 5F, and S7).

Given the benefits observed in CD28-based CAR-T cells against antigen-low cell lines[14] and the reported synergy seen in CAR-T cells containing the 4-1BB and CD28 co-stimulation in parallel,[38,39] we considered co-transducing CD28-based CARs with previously used 4-1BB co-stimulated ARI0001 and ARI0002h CARs. In assays against Ramos CD19 Low cells, single 4-1BB-based CAR-T cells displayed better cytotoxicity than CD28 CAR-T cells, favoring the co-transduced 4-1BBz and CD19-BBz/BCMA-CD28z products (Figure S8). Therefore, based on our clinical experience with ARI0002h and the limited advantage of BCMA-CD28z over BCMA-BBz, we opted to proceed with 4-1BB-based CARs for our dual-targeting strategies.

### ARI0003 therapy for NHL relapsed or refractory to anti-CD19 CAR-T cell treatment

We next explored whether treatment with dual-CAR-T cells might be beneficial in an NHL xenograft model of relapsed or refractory disease after CD19 CAR-T cell therapy. NSG mice implanted with Ramos CD19 Low cells were treated with control T cells or ARI0001 $CAR^+$-T cells (Figure 6A). Two weeks later, control T cell-treated mice showed disease recurrence, while ARI0001-treated mice exhibited heterogeneous responses (Figure 6B). Subsequently, ARI0001-treated mice were randomized into four groups for a second treatment of $CAR^+$-T cells: ARI0001, ARI0003, pooled CAR-T cells, or control T cells (Figure 6A). All treatments significantly extended

**Figure 4. ARI0003 shows enhanced functionality compared to other dual-targeting strategies**

(A) K652 cells were genetically modified to express truncated CD19, BCMA, or both antigens. CD19 and BCMA expressions were analyzed by flow cytometry. (B) The *in vitro* killing ability of the different strategies was analyzed after co-culture with K562 cells. Indicated target cells were co-cultured at an E:T ratio of 1:1 with CAR-T cells for 24 h. Specific lysis of cells expressing one or both antigens was measured in a luciferase-based killing assay. Bar graphs show the mean ± SD. Each point represents a healthy donor ($n = 3$). (C and D) The strength of interaction among all dual-targeting strategies with Ramos WT (C) or Ramos CD19 Low (D) target cells was measured. The percentage of total CAR-T cells remaining bound to target cells as the acoustic force ramp is applied from 0 to 1,000 pN is shown (left). The fold change of the percentage of bound CAR-T cells versus UTD T cells at 1,000 pN is shown (right). Data are presented as means ± SEMs from two donors in technical triplicate ($n = 2$). $p$ values were calculated using a one-way ANOVA test. $^*p < 0.05$; $^{**}p < 0.01$; $^{***}p < 0.001$. (E–H) Long-term cytotoxicity and proliferation of dual-targeting strategies. Control T and CAR-T cells were co-cultured with Ramos or Ramos CD19 Low for 7 days. (E) $CD3^+$ (T lymphocytes) and $GFP^+$ (tumor) populations after 7 days of co-culture in a representative healthy donor. (F) Quantification of the distribution of populations observed in (E). (G) T cell proliferation analyzed by flow cytometry. Each point represents a different experiment with a different healthy donor ($n = 2$). (H) Surface CAR expression levels across different $CAR^+$ populations on ARI0003 and pooled T cells, both before and after co-culture with the Ramos WT cell line at an E:T ratio of 1:4. Results were obtained from three distinct healthy donors ($n = 3$) and are presented as the mean ± SD. Statistical significance was evaluated using a one-way t test. $^*p < 0.05$.

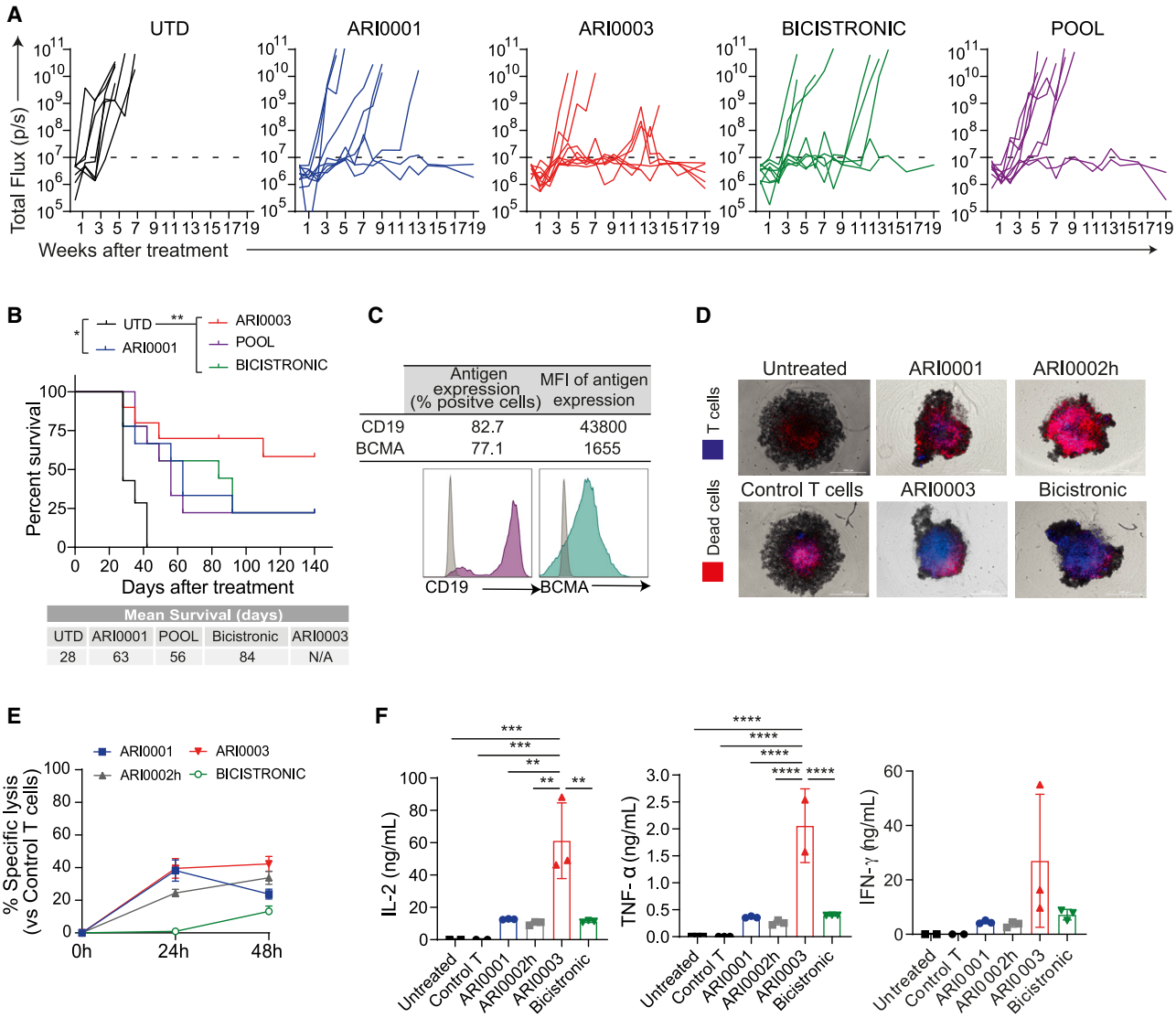


**Figure 5. Enhanced efficacy of ARI0003 in NSG mice and PDLS assays**

(A and B) ARI0003 *in vivo* antitumor activity in a "CAR-T limiting dose" Burkitt lymphoma xenograft model. NSG mice were i.v. inoculated with lymphoma cells expressing luciferase and treated 4 days later with $5 \times 10^5$ control T cells ($n = 7$), ARI0001 ($n = 9$), pooled CAR-T ($n = 9$), ARI0003 ($n = 10$), or bicistronic CAR-T cells ($n = 9$) (60% $CAR^+$-T cells for all groups). Disease progression was measured by bioluminescence photometry (IVIS). (A) Quantitative analysis of BLI as total flux (p/s) per individual animal in each group. (B) The Kaplan-Meier survival curves of treated mice are plotted and mean survival (days) calculated. Log rank (Mantel-Cox) test. (C–F) PDLS from a follicular lymphoma patient as a preclinical model to test ARI0003 CAR-T cells. (C) CD19 and BCMA antigen expression on PDLS before CAR-T cell co-culture analyzed by flow cytometry. (D) Images captured with Cytation 1 of representative PDLS that were formed for 4 days and then co-cultured with CAR-T cells for 2 more days. T cells are stained with CellTracker Violet (blue) and dead cells with propidium iodide (red). Loss of sphericity indicates CAR-T cell antitumor effect. (E) Specific killing of tumor spheroids by CAR-T cells overtime after co-culture at an E:T ratio of 1:2 as analyzed by flow cytometry. Data are presented as mean ± SD for triplicates. (F) Cytokine production by ELISA after 24-h co-culture at an E:T ratio of 1:2. Each dot in the ELISA represents a spheroid ($n = 3$). Two-way ANOVA test with Tukey's correction. $^{**}p < 0.01$; $^{***}p < 0.001$.

mice survival compared to the group initially treated with ARI0001 and re-treated with control T cells (Figure 6C). Disease stabilization was observed in animals re-treated with ARI0001 and pooled CAR-T cells, but relapse occurred in most animals around 4–5 weeks post-treatment (Figure 6B). Mice re-treated with ARI0003 exhibited a substantial decrease in disease signal (Figure 6D) and achieved complete disease elimination in six of the seven treated animals, maintaining malignancy-free status until the end of the experiment.

To further confirm ARI0003 reactivity against malignant B cells previously exposed to CD19 CAR-T cells, PDLS were generated from the samples of patients who relapsed after ARI0001 treatment. In a

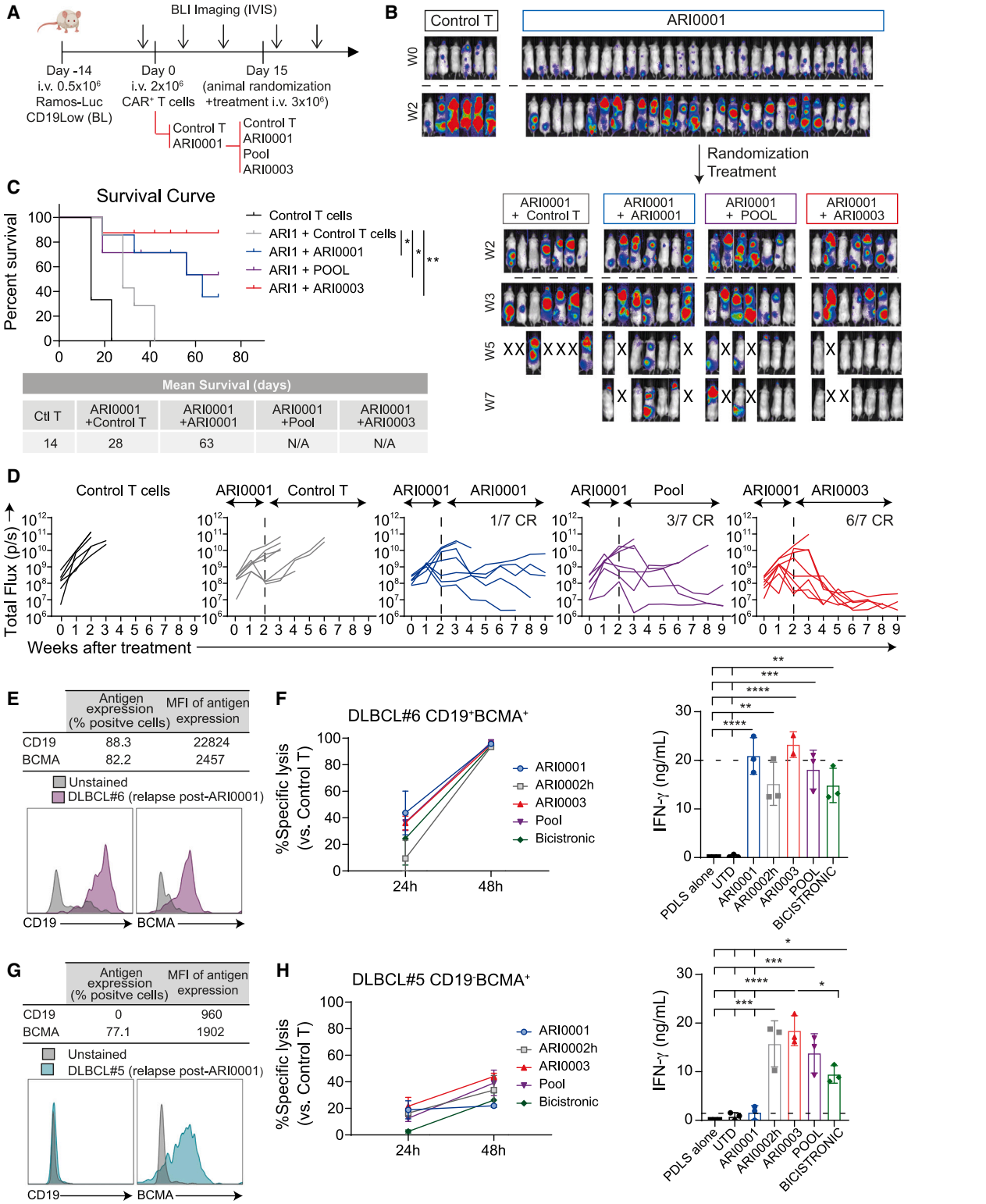


**Figure 6. ARI0003 as therapeutic option for NHL following relapse to CD19 CAR-T cell treatment**

(A–D) ARI0003 antitumor efficacy in a mouse model of NHL relapse following ARI0001 treatment. (A) Schematic representation of the experiment design. NSG mice were inoculated with lymphoma cells expressing low CD19 densities and treated with 2 × $10^6$ ARI0001 ($n$ = 28) or control T cells ($n$ = 6). Two weeks later, animals treated with

*(legend continued on next page)*

setting of a CD19$^+$ relapse (Figure 6E), all CAR-T cell effector groups, including ARI0001, could secrete cytokines and effectively target tumor cells (Figure 6F). Conversely, when co-cultured with PDLS from a patient who experienced a CD19$^-$ negative relapse (Figure 6G), only the BCMA CAR-T cells and dual-targeting strategies displayed activation (Figure 6H). Consistent with prior *in vivo* findings, and despite the low BCMA antigen densities in PDLS, ARI0003 cells retained activity against both CD19$^+$ and CD19$^-$ PDLS. These results highlight the therapeutic potential of ARI0003, not only as a primary treatment but also for relapsed or refractory NHL following CD19 CAR-T cell therapy.

### Co-transduction of CD19 and BCMA CARs outperforms the co-transduction of CD19 with CD20 or CD22 CARs

We next sought to head-to-head compare our product ARI0003 with previously reported dual-CARs co-targeting CD19 and CD20 or CD22.[40–42] To this end, we co-transduced ARI0001 with CD20-BBz (COTR CD19×20) or CD22-BBz (COTR CD19×22) CAR constructs (Figure 7A) and compared them against ARI0003. All groups displayed frequencies of CAR$^+$-T cells above 50% (Figure 7B), and co-transduction products showed comparable CAR expression frequencies (Figure S9).

To evaluate the functional capacity, we challenged monospecific and co-transduced CAR-T cells with Ramos CD19 Low. Ramos CD19 Low cells express low densities of CD22 (similar to CD19 and BCMA), while exhibiting higher CD20 antigen expression (Figure S4). In short-term cytotoxicity assays, all CAR-T groups successfully eliminated target cells, with superior activity of co-transduction groups over single CARs, especially at lower effector-to-target (E:T) ratios (Figure 7C). By contrast, long-term studies revealed that only ARI0003 was able to sustain tumor elimination, while monospecific CAR-T cells or the co-transduction of CD19×20 and CD19×22 failed to control tumor cell growth (Figures 7D and 7E). This enhanced long-term cytotoxicity of ARI0003 was accompanied by a significantly increased T cell proliferation only observed in this group (Figure 7F).

### Co-transduction is a feasible strategy to obtain clinical grade CD19/BCMA dual-CAR-T cells

To confirm the potential clinical translation of the co-transduction, five batches of ARI0003 cells were produced under GMP conditions using the CliniMACS prodigy system transducing T cells with MOI = 8 for ARI0001 and MOI = 2 for ARI0002h. The mean transduction efficiency was 50% of total CAR$^+$-T cells (Figure 8A). Within the CAR$^+$-T cell population, the production process achieved at least 20% double-positive CAR-T cells, meeting the product specifications that we had previously defined in the quality dossier of the investigational product presented to the regulatory agencies (Figure 8B). The cytotoxic activity *in vitro* against Ramos WT cells of these five batches of dual-CAR-T manufactured in GMP conditions was confirmed (Figure 8C). Additionally, we assessed the toxicity of ARI0003 in a panel of human healthy cells. We could not detect an increase in the toxicity profile of ARI0003 compared to ARI0001 or control T cells (untransduced [UTD]), while we observed activation with a HER2 CAR-T cell group used as a positive control (Figure S10). The similarity in safety profile to ARI0001 points to the potential of ARI0003 as a promising and safe therapeutic option for patients with NHL.

## DISCUSSION

Despite the encouraging results of CD19 CAR-T cells in NHL patients, a substantial percentage does not respond or relapses post-therapy. CD19 loss or downregulation is invoked as a key factor in relapse. Dual targeting, such as CD19 and CD22 or CD19 and CD20, aims to enhance efficacy, but early trials do not demonstrate improved outcomes compared to anti-CD19 CAR-T cells. Here, we report the optimization, preclinical development, and GMP manufacturing of ARI0003, a novel dual-CAR-T cell product targeting CD19 and BCMA for the treatment of NHL patients.

A key consideration in the development of dual-CAR-T cells is selecting optimal antigens. CD20, although brightly expressed in NHL, can be downregulated post-rituximab treatment.[43–45] CD22 is a challenging antigen to target due to its large structure, rigidity, substantial glycosylation, and low antigen densities, and it is downmodulated upon CAR targeting.[40,41,46,47] Given these challenges, we focused on co-targeting CD19 and BCMA. BCMA is expressed in most lymphoma cases, and NHL patients have not been previously exposed to treatments targeting this antigen.[25,48] In addition, CAR-T therapy targeting BCMA has been shown to be safe and effective in clinical trials,[26–28] and no BCMA loss has been detected in the first 60 multiple myeloma patients treated under a clinical trial with our academic anti-BCMA CAR, ARI0002h.[26,49]

To further support our decision to target BCMA alongside CD19—especially since BCMA is not a conventional lymphoma target—we compared our dual-targeting strategy with previously reported dual-CAR approaches that target CD19 and either CD20 or CD22.[40–42] Our findings show that the co-transduction product

ARI0001 received a second treatment consisting of 3 × 10$^6$ control T cells ($n$ = 7), ARI0001 ($n$ = 7), ARI0003 ($n$ = 7), or pooled ($n$ = 7) CAR-T cells (60% CAR$^+$ expression). Disease progression was measured by bioluminescence photometry (IVIS). (B) Mice pictures from the day before treatment to 7 weeks after treatment. (C) Kaplan-Meier survival curves for treated mice and mean survival (days). *$p$ < 0.05 and **$p$ < 0.005 by log rank (Mantel-Cox) test. (D) Quantitative analysis of BLI as total flux (p/s) per individual animals in each group. (E–H) PDLS from patients who relapsed after CD19-CAR-T cell therapy served as an *ex vivo* preclinical model to challenge CAR-T cells. (E and G) Histograms of CD19 and BCMA antigen expression on PDLS before CAR-T cell treatment, for CD19$^+$ and CD19$^-$ PDLS, respectively. (F and H) Specific killing of tumor cells of each CAR-T cell effector group after co-culture with CAR-T cells at an E:T ratio of 1:2 was compared to control T cells and analyzed by flow cytometry, for CD19$^+$ (F) and CD19$^-$ (H) PDLS, respectively. Data presented are mean ± SD for triplicates. IFN-γ production after 24-h co-culture at an E:T ratio of 1:2 was analyzed by ELISA in PDLS supernatant. Each dot in the ELISA corresponds to a spheroid ($n$ = 2–3).

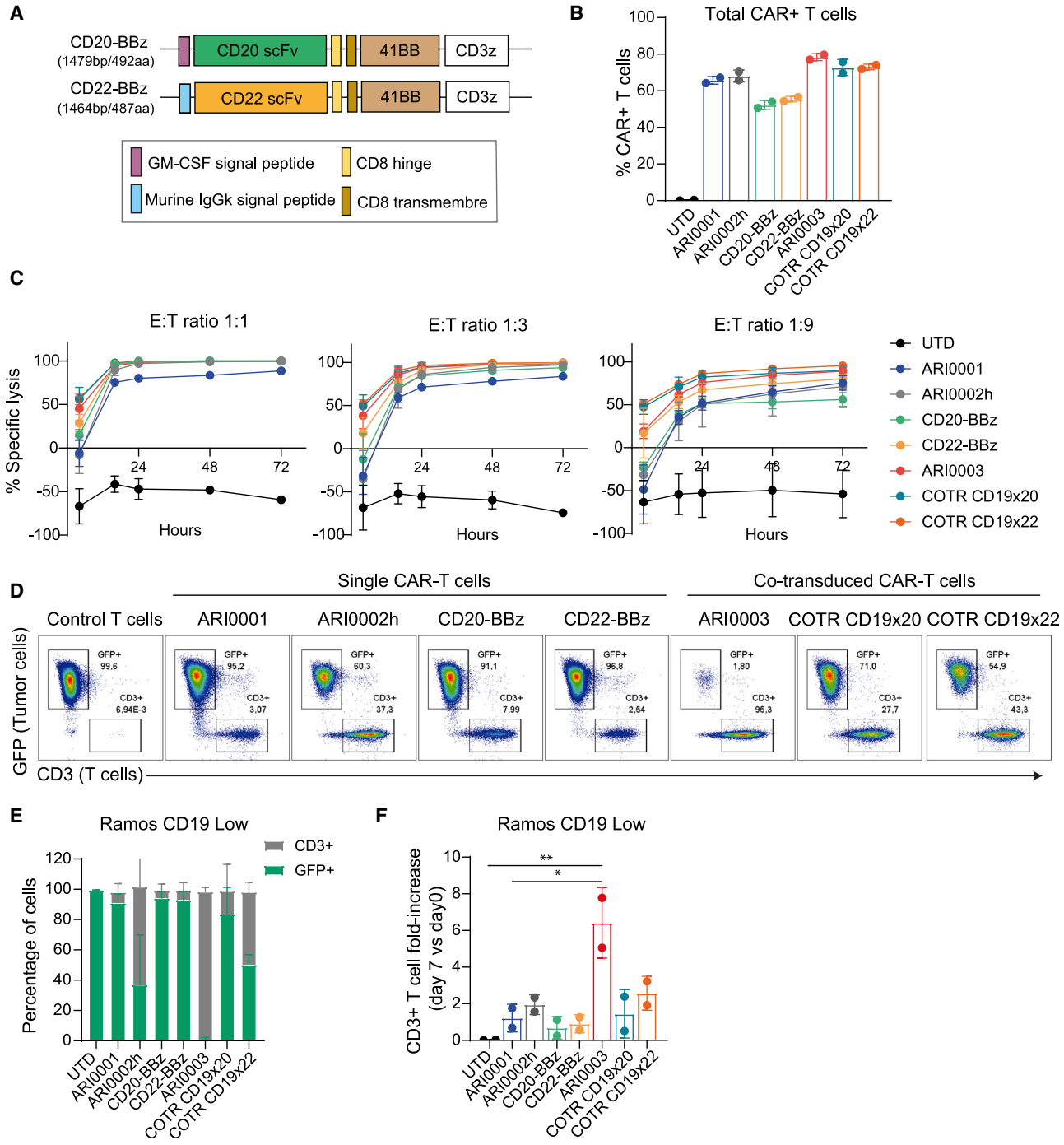


**Figure 7. CD19 and BCMA CAR co-transduction outperforms CD19 combined with CD20 or CD22 CARs**

(A) Schematic representation of CAR constructs. (B) The percentage of CAR-expressing T cells analyzed by flow cytometry is shown ($n$ = 2 healthy donors). (C) Monospecific CAR-T cells and dual-CAR-T cells were cultured with Ramos CD19 Low cells at indicated E:T ratios. Tumor cell lysis was evaluated over time using a BLI-based killing assay. Data represent the mean ± SD of triplicates from two healthy donors. (D–F) Long-term cytotoxicity and proliferation of single and dual-targeting CAR-T cell strategies. CAR-T cells were co-cultured with Ramos CD19 Low cells for 7 days ($n$ = 2 healthy donors). (D) Representative flow plots showing $CD3^+$ (T cells) and $GFP^+$ (tumor cells) populations. (E) Quantification of population distributions from (D). (F) T cell proliferation after 7 days of co-culture analyzed by flow cytometry. Bar graphs show the mean ± SD of the $CD3^+$ T cell fold-increase. Each point represents an experiment with a different healthy donor ($n$ = 2). $p$ Values were calculated using a one-way ANOVA test. $^{***}p \leq 0.001$, $^{**}p \leq 0.01$, $^{*}p \leq 0.05$

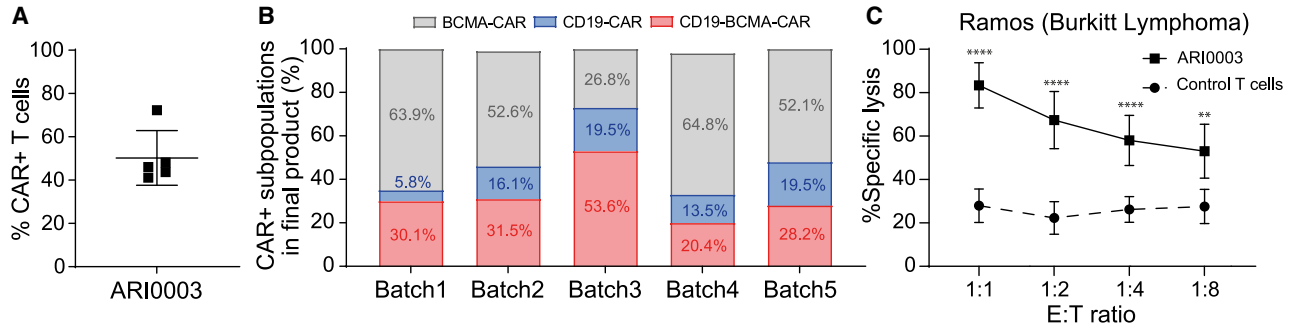


**Figure 8. Characterization of ARI0003 batches produced under GMP conditions**

(A) Percentage of CAR$^+$-T cells after transduction at clinical level analyzed by flow cytometry. Each dot represents an ARI0003 batch produced. (B) CAR distribution within the CAR$^+$ population of ARI0003. (C) ARI0003 cells were co-cultured with Ramos WT target cells at indicated E:T ratios. Lysis of the tumor cells was evaluated 24 h after co-culture by flow cytometry. Results represent the mean ± SD of $n = 5$ clinical grade manufactured products. Statistics in (C) were performed with multiple comparisons using two-way ANOVA. $^{**}p < 0.005$; $^{****}p < 0.0001$.

targeting both CD19 and BCMA provided a significant advantage in long-term tumor control compared to other co-transduction combinations. This result is particularly noteworthy, as CD20 and CD22 were more abundantly expressed in the panel of NHL tumor cells we examined. These findings suggest that certain scFvs may offer enhanced and sustained antitumor activity, highlighting the importance of both antigen selection and the choice of scFv for optimizing CAR-T cell efficacy. Here, we demonstrate that ARI0002h can effectively recognize low BCMA densities in NHL cells, inducing significant antitumor effects in models of NHL.

Dual targeting of BCMA and CD19 consistently resulted in enhanced control of NHL disease compared to single-targeted CAR-T cells, especially in models with low CD19 densities. This is particularly relevant considering recent reports pointing at low CD19 densities as a cause of refractory disease or poorer maintenance of ongoing responses after CD19-CAR-T cell treatment.[15,16]

Another consideration to address when developing dual-targeting CAR-T cells is balancing the expression of the two CARs in the T cell membrane to prevent a stronger antigen pressure on one target. Ideally, both CARs should be equally capable of recognizing their targeted antigens and eliciting a similar response in T cells. For instance, co-targeting with a CAR that exhibited stronger immune pressure on CD19 and inadequate activity on CD22 led to CD19$^-$ relapses but no CD22$^-$ relapses in the clinical setting.[15] When considering dual-targeting of CD19/BCMA, the favorable safety and efficacy results observed with ARI0001 and ARI0002h CAR-T cells in clinical trials provided encouragement to focus on developing the co-transduction product initially. However, co-transduced CARs, particularly the CD19-CAR, displayed significantly lower expression levels compared to individual transduction. The decrease in expression was more pronounced at higher MOIs, suggesting that the concurrent expression of multiple transgenes at elevated levels competes more intensely for the limited supply of resources involved in gene expression.[34] This observation was only seen when both LVs were co-transduced, since using the bicistronic construct resulted in a balanced expression of both CARs on the T cell membrane, in line with previous reports in the field.[50,51] This indicated that after CAR synthesis, both CARs could equally traffic to the T cell membrane and remained similarly stable.

While similar VCNs were observed in both single and co-transduction strategies, co-transduction resulted in lower RNA levels when transduced at a high MOI, suggesting that transgene load affects transcriptional machinery but does not fully explain the enhanced expression of the BCMA CAR compared to the CD19 CAR. The lack of increased CD19 CAR expression from codon-optimized constructs indicates that tRNA usage does not preferentially favor the BCMA CAR either, emphasizing the need to further investigate other cellular machinery that may play a more critical role in influencing transgene expression. Notably, a reduction in expression that may result in imbalanced CAR populations in dual-targeting strategies have already been observed by others in the field, although not addressed. Kokalaki et al.[47] observed a similar reduction in an anti-CD19 CAR expression when co-transduced with an anti-CD22 CAR. In a different approach, co-electroporation of equal amounts of two mRNAs encoding for cytokines in T cells resulted in the diminished expression of each protein, underscoring the significance of post-transcriptional machinery in transgene competition.[52] By using unequal MOIs of the two LVs, we have been able to obtain a final dual-CAR-T cell product with balanced expression of the two CARs.

In our study, the co-transduction of two LVs allowed the generation of CAR-T cells using lower vector copies per genome compared to the bicistronic, tandem, and loop dual-CAR-T cells. This is especially relevant after the release of a report by the US Food and Drug Administration indicating that T cell malignancies may occur following treatment with BCMA- and CD19-directed CAR-T cells. While a direct causal relationship between CAR insertion in the context of LVs and malignant transformation has not yet been identified, reducing the VCNs per cell may be important to mitigate the risk of genotoxicity.

For tandem and loop CAR design, crucial parameters impacting full functionality include extracellular region length, the scFv order, and

linker selection binding the two scFvs.[20] Typically, these parameters are empirically combined to identify the best candidate, requiring testing of various CAR constructs. Here, we conducted a structural prediction analysis that revealed that in some of the tandem designs, the scFvs could interact with one another, leading to competition with their respective binders. Notably, only the more rigid linkers of Tandem4 and Loop2 effectively prevented this undesired interaction. This prediction was in line with our functional studies, which demonstrated that only these two constructs had killing efficacy similar to ARI0002h against BCMA-expressing cells and ARI0001 against CD19-expressing cells. These results emphasize the importance of structural predictions in optimizing CAR constructs and provide a solid framework for future screening efforts.

Analysis of T cell functionality indicated that using separate CARs for CD19 and BCMA was more effective than a single CAR with dual specificities. This may be partly due to the lower stability of dual-targeting CAR molecules on the T cell membrane, suggested by the intracellular presence of a fraction of tandem and loop CAR molecules. Additionally, the observed reduction of the double-positive CAR population in ARI0003 during prolonged co-culture experiments in favor of monospecific CAR populations may indicate that dual-targeting T cells undergo exhaustion more rapidly and are depleted over time, consistent with previous reports.[53] This could partially account for the inability of the bicistronic, tandem, and loop CAR constructs to sustain long-term tumor elimination. Despite this, given that all strategies are effective at eliminating tumor cells in short-term experiments and that ARI0003, tandem, and loop constructs exhibit high avidity, the dual-targeting population appears to offer an initial advantage that may account for the superior long-term performance of ARI0003 compared to the pool strategy. However, the ideal dual-targeting strategy must yet be defined for each scFv combination, as different groups have reported different results with dual candidates.[17]

A major challenge to overcome in the field of CAR-T therapies is the difficult access to these costly treatments for most of the patients worldwide. Preclinical and clinical development of academic CARTs might alleviate this situation. ARI0001 and ARI0002h were approved by the Spanish Agency of Medicines and Medical Devices under the Hospital Exemption (HE) clause (RD 477/2014) in February 2021 and August 2024, respectively. The HE allows medicinal products manufactured on a non-industrial basis to become available for patients meeting the indication and is refunded by the health system. HE might be considered to be an intermediate step before requesting a centralized marketing authorization by the European Medicines Agency.[54] Based on the preclinical characterization of ARI0003 and our previous experience with academic CAR-T cells, we have opened a first-in-human, pilot, open-label, multicenter, non-randomized phase 1 clinical trial to test the safety and efficacy of ARI0003 in patients with r/r B cell aggressive lymphoma (CARTD-BG-01; clinicaltrials.gov ID: NCT06097455; EU Clinical Trial ID: 2023-5072-13-97-00), both as first CART therapy and for patients relapsing after a previous CART19.

## MATERIALS AND METHODS

### Isolation, transduction, and primary T cell expansion

Human T cells were isolated from healthy donor buffy coats purchased from Banc de Sang i Teixits, following approved institutional review board protocols. CAR-T cells were generated and expanded, as previously described.[55] Briefly, $CD4^+$ and $CD8^+$ T cells were isolated from peripheral blood using RosetteSep Kits (Stem Cell Technologies). T cells were stimulated with anti-CD3/CD28 magnetic beads (Invitrogen) and transduced by LVs at indicated MOIs. Interleukin-7 (IL-7) and IL-15 (Miltenyi) were added daily to a final concentration of 10 ng/mL. CAR-T cell products were mixed to a final 1:1 ($CD4^+$:$CD8^+$) ratio and normalized for CAR expression at day 10 before cryopreservation. T cells were cultured in RPMI-1640 supplemented with 10% of fetal bovine serum (FBS), penicillin/streptomycin (P/S) (100 mg/mL), 10 mM GlutaMAX, and 10 mM HEPES.

### CAR construction and lentivirus production

All CAR sequences were cloned into the pCCL third-generation LV with EF1 promoter. CARs targeting CD19 (ARI0001) and BCMA (ARI0002h) have been previously described.[29,30] For the CD28z-based versions, a BCMA-28z CAR was synthesized flanked by XmaI and NheI, and the CD19 CAR was then cloned into the CD28z backbone. All dual-CAR receptors were designed to contain the scFv from ARI0001 with the CD8α leader and the scFv from ARI0002h with the Ig kappa chain leader. The sequence of the leader for each construct is determined based on the scFv placed in the distal position. All dual-CAR receptors were designed to contain the scFv from ARI0001 with the CD8α leader and the scFv from ARI0002h with the Ig kappa chain leader. The sequence of the leader for each construct is determined based on the scFv placed in the distal position. Tandem and loop CAR extracellular domains were custom synthesized (GenScript) and cloned into the ARI0001 backbone. Bicistronic CAR was *de novo* synthesized for codon optimization of the intracellular repeated sequences to prevent DNA recombination, using GenScript's codon optimization tool. scFvs used for targeting CD20 (Leu16), CD22 (m971), and anti-HER2 (4D5-5) or anti-mesothelin (M11) CARs were described previously.[40,42,56] CD20-BBz includes the murine Ig heavy-chain leader peptide, while CD22-BBz uses the human GM-CSFR signal peptide. All CAR constructs used in this study incorporate the CD8α extracellular spacer region and transmembrane along with the 4-1BB co-stimulation and the CD3z endodomains, unless otherwise indicated. The plasmid coding for GFP-FireFlyLuciferase (GFP-FFLuc) was kindly provided by Dr. Amer Najjar.

LVs were produced as previously described.[57] Briefly, 293FTs were transfected with pCCL transfer plasmid, and a packaging mix containing a plasmid for the viral RNA (pREV), a plasmid encoding the Rev response element (pRRE), and a plasmid containing the vesicular stomatitis virsu (pVSV) using polyethylenimine (Polysciences). The supernatant was harvested at 48 and 72 h and concentrated with LentiX following the manufacturer's protocol (Clontech). Viral titers (transducing units per milliliter) were calculated based on protein expression levels as follows: ((total number of cells/100) × (percentage of

transduced cells) × dilution of the virus supernatant). The dilution used was the one at which approximately 10%–30% of the cells were positive for CAR expression.

### Cell lines

Tumor cell lines were acquired from the American Tissue Culture Collection and regularly validated to be *Mycoplasma* free. The Ramos CD19 Low cell line was generated with CRISPR-Cas9 technology, knocking out *CD19* from Ramos WT and overexpressing it under a weak promoter (PGK100).[9] Cell lines were cultured in RPMI-1640 supplemented with 10% FBS and P/S (100 mg/mL), except for U266 cells, which were cultured with 15% FBS. Cell lines were maintained at 37°C with 5% $CO_2$. Cells expressing CD19, BCMA, or GFP-FFLuc were generated through lentiviral transduction.

### Flow cytometry

The following antibodies were used for lymphocyte staining: CD4 (phycoerythrin [PE], OKT4, Invitrogen), CD8 (fluorescein isothiocyanate, RPA-T8, BioLegend), CD45 (PerCP-Cy5.5, HI3, BD Biosciences), and CD3 (PerCP-EF710, OKT3, Invitrogen). The following antibodies were used for tumor cell staining: CD19 (PE-Cy7, SJ25C1, BD Biosciences), CD19 (APC, HIB19, BD), BCMA (AF647, 19F2, Biolegend), CD20 (2H7, BD Biosciences), CD22 (HIB22, BD Biosciences). Data acquisition was performed using FACSCanto II or Fortessa5L (BD Biosciences) and analyzed with FlowJo Software (version 10, TreeStar).

### CAR detection

For anti-CD19, anti-BCMA, and anti-CD22 CAR surface detection, cells were stained using human recombinant proteins CD19-Fc (R&D Systems) and BCMA or CD22-polyhistidine tag (SinoBiological), followed by an anti-Fc-BV421 or anti-His-APC (both from BioLegend) secondary antibodies. CD20 CAR expression was assessed using a biotin-SP-AffiniPure F(ab)′2 fragment-specific goat anti-mouse IgG antibody (Jackson ImmunoResearch), followed by incubation with streptavidin-PE (BD Biosciences). Intracellular staining was performed using the Intracellular Fixation & Permeabilization Buffer Set (Thermo Fisher), following the manufacturer's instructions.

### Surface density of CAR molecules

The number of CAR molecules on the CAR-T cell surface was quantified using BD Quantibrite beads, following the manufacturer's protocol (BD Biosciences, lot 02587). Human PE-labeled recombinant proteins CD19-His Tag (Acro Biosystems) and BCMA-His Tag (Acro Biosystems) were used. Samples were analyzed using FACSCanto 5L cytometer. FlowJo software was used to create a standard curve from bead fluorescence, and the CAR molecule count per cell was determined by comparing the fluorescence intensity of the CAR-T cells to that of the beads.

### qPCR for LV insertion copy number determination

Genomic DNA was extracted from $CD4^+$ CAR-T cells after 6 or 8 days of expansion using the DNeasy Blood & Tissue Kit (Qiagen). Following extraction, DNA samples were quantified with a NanoDrop spectrophotometer and diluted to a concentration of 25–100 ng/μL. For each sample, 100 ng genomic DNA was amplified. qPCR was performed using the LightCycler 480 SYBR Green I Master mix (Roche) and custom primers (10 μM, Integrated DNA Technologies) targeting woodchuck hepatitis virus post-transcriptional regulatory element (WPRE), GATA, anti-CD19 scFv, or anti-BCMA scFv. Standard curves for each gene were generated, ranging from $10^8$ to $10^2$ copies per genome. The reactions were carried out in 384-well plates (Roche) on a LightCycler 480 system (Roche), with cycling conditions consisting of an initial denaturation at 95°C for 5 min, followed by 40 cycles of amplification (95°C for 10 s, 58°C for 10 s, and 72°C for 5 s). The Ct values were calculated using the LightCycler software and normalized to the GATA reference gene. All samples, including those used for standard curves, were analyzed in duplicate. WPRE or scFv quantification was employed to assess the total number of CAR molecules per sample, with UTD T cells serving as the negative control for CAR expression.

### Real-time PCR for mRNA quantification

Total RNA was extracted from $CD4^+$ CAR-T cells on day 6 or 8 of expansion using the RNeasy Micro Kit (Qiagen). cDNA synthesis was performed using the High-Capacity RNA-to-cDNA Kit (Thermo Fisher). Real-time PCR was conducted with the TaqMan Gene Expression Master Mix (Thermo Fisher) and custom TaqMan Gene Expression Assays (Thermo Fisher) targeting Actin-B, anti-CD19 scFv, or anti-BCMA scFv. For each sample, 100 ng cDNA was used for PCR amplification in 384-well plates (Thermo Fisher) on the Applied Biosystems 7900 Real-Time PCR System. The cycling conditions included an initial incubation at 50°C for 2 min, followed by a denaturation step at 95°C for 10 min. Amplification was carried out over 40 cycles of 95°C for 15 s and 60°C for 1 min. The Ct values for CD19 and BCMA were normalized to the housekeeping gene Actin-B.

### CAR-T cell functional studies

CAR-T cells were co-cultured with luciferase-expressing target cells. For luciferase-based killing assays, the luciferase signal was determined using a synergy HT Plate Reader (BioTek) within 10 min after the addition of D-luciferin (20 mg/mL; PerkinElmer). Specific lysis calculation is as follows: % Specific lysis = [1 – (BLI signal in treated wells/BLI signal in untreated wells)] × 100% (BLI, bioluminescence imaging). Cytokine concentration in the culture supernatant was measured with the ELISA Max Deluxe Set (BioLegend).

For proliferation assays, CAR-T cells and GFP-expressing target cells were co-cultured for 7 days. The total number of T cells and tumor cells was calculated by flow cytometry using CountBright Absolute Counting Beads (Thermo Fisher) according to the manufacturer's instructions.

To analyze the enrichment of $CAR^+$ populations, T cells were co-cultured with target cells at an E:T ratio of 1:4. After 7 days of

co-culture, $CD3^+GFP^-$ cells were sorted, rested in fresh R10 media supplemented with IL-15 (20 ng/mL) for 24 h, and then analyzed for surface and intracellular CAR expression using flow cytometry. Cell sorting was performed using an FACSAria II Cytometer (BD Biosciences).

### Cell-binding avidity assays

Ramos WT or Ramos CD19 Low were seeded at a density of $150^6$ cells/mL on poly-L-lysine-coated chips for 2 h at 37°C. Thawed and overnight rested T cells were stained with CellTrace Far Red Cell Proliferation Kit (Thermo Scientific, C34564) according to the manufacturer's instructions. CAR-T cells were normalized for transduction efficiency and bound for 10 min prior to force application using the z-Movi Cell Avidity Analyzer (Lumicks). Experiments were performed in triplicate and with UTD or CAR-T cells from at least two different healthy donors. The order of effector cell addition was randomized between different chips. Data analysis was performed using Oceon software version 1.2.8 and statistics were assessed by GraphPad Prism version 9.4.1.

### Structural prediction analysis

Structural models were produced with AlphaFold3, using as input sequences the extracellular motifs (CD hinge and scFv) and excluding chain and signal leaders. All predictions yielded average pLDDT values over 70.[58]

### PDLS generation and CAR-T cell treatment

PDLS generation from primary samples have been previously described.[59] For co-culture experiments, FL or DLBCL samples were thawed in sterile conditions and resuspended in enriched medium (EM). Primary samples were mixed with monocytes at a 4:1 ratio and cultured in Nunclon SpheraTM 96-well Ultra-Low Attachment microplates (Thermo Fisher) and EM supplemented with CD40L, IL-21, and IL-4. PDLS were maintained at 37°C, 5% $CO_2$ for 4 days and assessed for CD19 and BCMA expression by flow cytometry. Four days after culture, CAR-T cells were added at different E:T ratios and co-cultured for 24–72 h. To determine the cell number of viable cells, disaggregated PDLS were analyzed reading a fix volume using a high-throughput sampler (HTS) integrated in the cytometer using specific population markers (CD20 and CD3) together with the viability dye LIVE/DEAD Aqua (Thermo Fisher). PDLS were mechanically disaggregated at indicated time points and analyzed by flow cytometry (LSRFortessa SORP-HTS, BD Biosciences).

### NHL xenograft studies in NSG mice and bioluminescence imaging

Animal studies were approved by the Ethics Committee for Animal Experimentation at the University of Barcelona and Generalitat de Catalunya. Male or female immunodeficient NSG mice, aged 8–12 weeks, were intravenously (i.v.) injected with $5 \times 10^5$ tumor cells expressing GFP-FFLuc. Prior to treatment, mice were randomized. Disease progression was monitored weekly using BLI with the Xenogen IVIS 200 Imaging System (PerkinElmer). Data analysis was performed using Living Image software (PerkinElmer). For survival studies, mice were sacrificed upon reaching a total flux value of $\geq 1 \times 10^{10}$ photons per second (p/s).

### GMP-grade batch production of ARI0003

LV particles were produced in a cleanroom facility following GMP guidelines.[29] Clinical GMP-grade ARI0003 cells were produced using the CliniMACS Prodigy system (Miltenyi) as previously described.[29,30] Briefly, CD4/CD8 T cells were selected from patients' leukapheresis, stimulated and co-transduced with indicated MOI of both ARI0001 and ARI0002h lentiviruses, and expanded in TexMACs media supplemented with IL-7 and IL-15 (Miltenyi) until a dose of $3.5 \times 10^8$ $CAR^+$-T cells was achieved.

### Statistical analysis

All statistical analyses were performed using GraphPad Prism version 9.4.1 as detailed in the figure legends. See supplemental methods for more details.

## DATA AND CODE AVAILABILITY

The datasets generated and/or analyzed during the present study are available from the corresponding author on reasonable request.

## ACKNOWLEDGMENTS

This study was supported by research funding from "'la Caixa" Foundation to M.J. (LCF/PR/SP23/52950004); the Spanish Ministry of Science and Innovation under a Ramon y Cajal grant RYC2018-024442-I to S.G. and PID2020-119692RB-C22 to C.F.; the Innovative Medicines Initiative 2 Joint Undertaking under grant agreement no. 116026 to S.G. (this joint undertaking receives support from the European Union's Horizon 2020 research and innovation program and European Federation of Pharmaceutical Industries and Associations), the Spanish Association Against Cancer (INVES222988RODR to A.R.-G.), and the AGAUR_INVESTIGO22 100028TC1 grant, within the framework of the Recovery, Transformation, and Resilience Plan, funded by the European Union's NextGenerationEU Recovery Mechanism. C.D.-L. was supported by a personal "Formación de personal investigador" fellowship from the Ministry of Economy and competitiveness (PRE2018-083797) associated with the project SAF2017-88275-R to P.P.-G. We also thank the Generalitat de Catalunya for support (AGAUR 2021-SGR-01294) to P.P.-G. M.O.-M. was granted a "Formacion para investigadores en el ámbito de la Investigacin sanitaria" predoctoral training grant (IFI18/00035). B.M.-A. was supported by the Miguel Servet program (grant no. CP21/00111) of the Institute of Health Carlos III. We also acknowledge the support of the CERCA Programme/Generalitat de Catalunya. This work was developed at the Centro Esther Koplowitz, Barcelona, Spain. We thank the Flow Cytometry and Cell Sorting core facility of Fundació de Recerca Clínic Barcelona-Institut d'Investigacions Biomèdiques August Pi Sunyer (FRCB-IDIBAPS) for their technical help. We also thank the animal facility of the University of Barcelona.

## AUTHOR CONTRIBUTIONS

M.B., N.B.-G., and A.R.-G. performed experiments, analyzed and interpreted the data, and wrote the manuscript. L.A. produced the ARI0003 batches under GMP conditions and analyzed the data. C.B.-L. performed the experiments with PDLS and analyzed the data. M.G.-A. performed experiments including lentiviral production and viral copy number determination. J.C. performed *in vivo* experiments. M.O.-M. performed the codon usage experiments with codon-optimized construct versions. A.A.-V. generated the Ramos CD19 Low cell line. M.E.-R. and M.P. supervised the ARI0003 batches under GMP conditions. N.F. performed the structural predictions. M.J. provided conceptual guidance. B.M.-A. performed previous experiments that served as background for this study. X.M.A. and C.F. provided conceptual guidance on co-transduction experiments, codon optimization, and transgene expression. J.D., E.O., and G.C. helped with the clinical trial design and provided conceptual and regulatory guidance. P.P.-G. provided conceptual guidance on the pre-clinical models. A.U.-I. identified unmet medical needs, provided conceptual guidance, and wrote the manuscript. S.G. supervised the project, including the design of the experiments, the data analysis, and wrote the manuscript. All authors revised the manuscript.

## DECLARATION OF INTERESTS

S.G. is an inventor on patents related to CAR-T cell therapy, filed by the University of Pennsylvania and licensed to Novartis and Tmunity Therapeutics, and has received commercial research funding from Gilead. A.R.-G. is an inventor on patents related to CAR-T cell therapy, filed by the University of Pennsylvania. M.P., M.J., J.D., and A.U.-I. are inventors of a patent describing ARI0001. B.M.-A., A.U.-I., and M.J. are inventors of a patent describing ARI0002h.

## DECLARATION OF GENERATIVE AI AND AI-ASSISTED TECHNOLOGIES IN THE WRITING PROCESS

During the preparation of this work the author(s) used ChatGTP to check some parts of the text for spelling and grammar errors. After using this tool, the author(s) reviewed and edited the content as needed and take(s) full responsibility for the content of the publication.

## SUPPLEMENTAL INFORMATION

Supplemental information can be found online at https://doi.org/10.1016/j.ymthe.2024.11.028.

## REFERENCES


1. Maude, S.L., Laetsch, T.W., Buechner, J., Rives, S., Boyer, M., Bittencourt, H., Bader, P., Verneris, M.R., Stefanski, H.E., Myers, G.D., et al. (2018). Tisagenlecleucel in Children and Young Adults with B-Cell Lymphoblastic Leukemia. N. Engl. J. Med. *378*, 439–448.
2. Shah, B.D., Ghobadi, A., Oluwole, O.O., Logan, A.C., Boissel, N., Cassaday, R.D., Leguay, T., Bishop, M.R., Topp, M.S., Tzachanis, D., et al. (2021). KTE-X19 for relapsed or refractory adult B-cell acute lymphoblastic leukaemia: phase 2 results of the single-arm, open-label, multicentre ZUMA-3 study. The Lancet *398*, 491–502.
3. Neelapu, S.S., Locke, F.L., Bartlett, N.L., Lekakis, L.J., Miklos, D.B., Jacobson, C.A., Braunschweig, I., Oluwole, O.O., Siddiqi, T., Lin, Y., et al. (2017). Axicabtagene Ciloleucel CAR T-Cell Therapy in Refractory Large B-Cell Lymphoma. N. Engl. J. Med. *377*, 2531–2544.
4. Schuster, S.J., Bishop, M.R., Tam, C.S., Waller, E.K., Borchmann, P., McGuirk, J.P., Jäger, U., Jaglowski, S., Andreadis, C., Westin, J.R., et al. (2019). Tisagenlecleucel in Adult Relapsed or Refractory Diffuse Large B-Cell Lymphoma. N. Engl. J. Med. *380*, 45–56.
5. Abramson, J.S., Palomba, M.L., Gordon, L.I., Lunning, M.A., Wang, M., Arnason, J., Mehta, A., Purev, E., Maloney, D.G., Andreadis, C., et al. (2020). Lisocabtagene maraleucel for patients with relapsed or refractory large B-cell lymphomas (TRANSCEND NHL 001): a multicentre seamless design study. The Lancet *396*, 839–852.
6. Wang, M., Munoz, J., Goy, A., Locke, F.L., Jacobson, C.A., Hill, B.T., Timmerman, J.M., Holmes, H., Jaglowski, S., Flinn, I.W., et al. (2020). KTE-X19 CAR T-Cell Therapy in Relapsed or Refractory Mantle-Cell Lymphoma. N. Engl. J. Med. *382*, 1331–1342.
7. Locke, F.L., Miklos, D.B., Jacobson, C.A., Perales, M.A., Kersten, M.J., Oluwole, O.O., Ghobadi, A., Rapoport, A.P., McGuirk, J., Pagel, J.M., et al. (2022). Axicabtagene Ciloleucel as Second-Line Therapy for Large B-Cell Lymphoma. N. Engl. J. Med. *386*, 640–654.
8. Abramson, J.S., Solomon, S.R., Arnason, J., Johnston, P.B., Glass, B., Bachanova, V., Ibrahimi, S., Mielke, S., Mutsaers, P., Hernandez-Ilizaliturri, F., et al. (2023). Lisocabtagene maraleucel as second-line therapy for large B-cell lymphoma: primary analysis of the phase 3 TRANSFORM study. Blood *141*, 1675–1684.
9. Ando, Y., Siegler, E.L., Ta, H.P., Cinay, G.E., Zhou, H., Gorrell, K.A., Au, H., Jarvis, B.M., Wang, P., and Shen, K. (2019). Evaluating CAR-T Cell Therapy in a Hypoxic 3D Tumor Model. Adv. Healthc. Mater. *8*, 1900001.
10. Maude, S.L., Frey, N., Shaw, P.A., Aplenc, R., Barrett, D.M., Bunin, N.J., Chew, A., Gonzalez, V.E., Zheng, Z., Lacey, S.F., et al. (2014). Chimeric antigen receptor T cells for sustained remissions in leukemia. N. Engl. J. Med. *371*, 1507–1517.
11. Shah, N.N., Lee, D.W., Yates, B., Yuan, C.M., Shalabi, H., Martin, S., Wolters, P.L., Steinberg, S.M., Baker, E.H., Delbrook, C.P., et al. (2021). Long-Term Follow-Up of CD19-CAR T-Cell Therapy in Children and Young Adults With B-ALL. J. Clin. Oncol. *39*, 1650–1659.
12. Park, J.H., Rivière, I., Gonen, M., Wang, X., Sénéchal, B., Curran, K.J., Sauter, C., Wang, Y., Santomasso, B., Mead, E., et al. (2018). Long-Term Follow-up of CD19 CAR Therapy in Acute Lymphoblastic Leukemia. N. Engl. J. Med. Overseas. Ed. *378*, 449–459.
13. Plaks, V., Rossi, J.M., Chou, J., Wang, L., Poddar, S., Han, G., Wang, Z., Kuang, S.Q., Chu, F., Davis, R.E., et al. (2021). CD19 target evasion as a mechanism of relapse in large B-cell lymphoma treated with axicabtagene ciloleucel. Blood *138*, 1081–1085.
14. Majzner, R.G., Rietberg, S.P., Sotillo, E., Dong, R., Vachharajani, V.T., Labanieh, L., Myklebust, J.H., Kadapakkam, M., Weber, E.W., Tousley, A.M., et al. (2020). Tuning the Antigen Density Requirement for CAR T-cell Activity. Cancer Discov. *10*, 702–723.
15. Spiegel, J.Y., Patel, S., Muffly, L., Hossain, N.M., Oak, J., Baird, J.H., Frank, M.J., Shiraz, P., Sahaf, B., Craig, J., et al. (2021). CAR T cells with dual targeting of CD19 and CD22 in adult patients with recurrent or refractory B cell malignancies: a phase 1 trial. Nat. Med. *27*, 1419–1431.
16. Locke, F.L., Filosto, S., Chou, J., Vardhanabhuti, S., Perbost, R., Dreger, P., Hill, B.T., Lee, C., Zinzani, P.L., Kröger, N., et al. (2024). Impact of tumor microenvironment on efficacy of anti-CD19 CAR T cell therapy or chemotherapy and transplant in large B cell lymphoma. Nat. Med. *30*, 507–518.
17. Brillembourg, H., Martinez-Cibrian, N., Bachiller, M., Alserawan, L., Ortiz-Maldonado, V., Guedan, S., and Delgado, J. (2024). The role of chimeric antigen receptor T cells targeting more than one antigen in the treatment of B-cell malignancies. Br. J. Haematol. *204*, 1649–1659.
18. Zah, E., Lin, M.Y., Silva-Benedict, A., Jensen, M.C., and Chen, Y.Y. (2016). T Cells Expressing CD19/CD20 Bispecific Chimeric Antigen Receptors Prevent Antigen Escape by Malignant B Cells. Cancer Immunol. Res. *4*, 498–508.
19. Wei, G., Zhang, Y., Zhao, H., Wang, Y., Liu, Y., Liang, B., Wang, X., Xu, H., Cui, J., Wu, W., et al. (2021). CD19/CD22 Dual-Targeted CAR T-cell Therapy for Relapsed/Refractory Aggressive B-cell Lymphoma: A Safety and Efficacy Study. Cancer Immunol. Res. *9*, 1061–1070.
20. Tong, C., Zhang, Y., Liu, Y., Ji, X., Zhang, W., Guo, Y., Han, X., Ti, D., Dai, H., Wang, C., et al. (2020). Optimized tandem CD19/CD20 CAR-engineered T cells in refractory/relapsed B-cell lymphoma. Blood *136*, 1632–1644.
21. Wang, T., Tang, Y., Cai, J., Wan, X., Hu, S., Lu, X., Xie, Z., Qiao, X., Jiang, H., Shao, J., et al. (2023). Coadministration of CD19- and CD22-Directed Chimeric Antigen Receptor T-Cell Therapy in Childhood B-Cell Acute Lymphoblastic Leukemia: A Single-Arm, Multicenter, Phase II Trial. J. Clin. Oncol. *41*, 1670–1683.
22. Wang, N., Hu, X., Cao, W., Li, C., Xiao, Y., Cao, Y., Gu, C., Zhang, S., Chen, L., Cheng, J., et al. (2020). Efficacy and safety of CAR19/22 T-cell cocktail therapy in patients with refractory/relapsed B-cell malignancies. Blood *135*, 17–27.
23. Cordoba, S., Onuoha, S., Thomas, S., Pignataro, D.S., Hough, R., Ghorashian, S., Vora, A., Bonney, D., Veys, P., Rao, K., et al. (2021). CAR T cells with dual targeting of CD19 and CD22 in pediatric and young adult patients with relapsed or refractory B cell acute lymphoblastic leukemia: a phase 1 trial. Nat. Med. *27*, 1797–1805.
24. Dogan, A., Siegel, D., Tran, N., Fu, A., Fowler, J., Belani, R., and Landgren, O. (2020). B-cell maturation antigen expression across hematologic cancers: a systematic literature review. Blood Cancer J. *10*, 73.
25. Bluhm, J., Kieback, E., Marino, S.F., Oden, F., Westermann, J., Chmielewski, M., Abken, H., Uckert, W., Höpken, U.E., and Rehm, A. (2018). CAR T Cells with Enhanced Sensitivity to B Cell Maturation Antigen for the Targeting of B Cell Non-Hodgkin's Lymphoma and Multiple Myeloma. Mol. Ther. *26*, 1906–1920.
26. Oliver-Caldés, A., González-Calle, V., Cabañas, V., Español-Rego, M., Rodríguez-Otero, P., Reguera, J.L., López-Corral, L., Martin-Antonio, B., Zabaleta, A., Inogés, S., et al. (2023). Fractionated initial infusion and booster dose of ARI0002h, a humanised, BCMA-directed CAR T-cell therapy, for patients with relapsed or refractory multiple myeloma (CARTBCMA-HCB-01): a single-arm, multicentre, academic pilot study. Lancet Oncol. *24*, 913–924.
27. Munshi, N.C., Anderson, L.D., Jr., Shah, N., Madduri, D., Berdeja, J., Lonial, S., Raje, N., Lin, Y., Siegel, D., Oriol, A., et al. (2021). Idecabtagene Vicleucel in Relapsed and Refractory Multiple Myeloma. N. Engl. J. Med. *384*, 705–716.
28. Berdeja, J.G., Madduri, D., Usmani, S.Z., Jakubowiak, A., Agha, M., Cohen, A.D., Stewart, A.K., Hari, P., Htut, M., Lesokhin, A., et al. (2021). Ciltacabtagene autoleucel, a B-cell maturation antigen-directed chimeric antigen receptor T-cell therapy in

patients with relapsed or refractory multiple myeloma (CARTITUDE-1): a phase 1b/2 open-label study. The Lancet *398*, 314–324.

29. Castella, M., Boronat, A., Martín-Ibáñez, R., Rodríguez, V., Suñé, G., Caballero, M., Marzal, B., Pérez-Amill, L., Martín-Antonio, B., Castaño, J., et al. (2019). Development of a Novel Anti-CD19 Chimeric Antigen Receptor: A Paradigm for an Affordable CAR T Cell Production at Academic Institutions. Mol. Ther. Methods Clin. Dev. *12*, 134–144.
30. Perez-Amill, L., Suñe, G., Antoñana-Vildosola, A., Castella, M., Najjar, A., Bonet, J., Fernández-Fuentes, N., Inogés, S., López, A., Bueno, C., et al. (2021). Preclinical development of a humanized chimeric antigen receptor against B cell maturation antigen for multiple myeloma. Haematologica *106*, 173–184.
31. Ortíz-Maldonado, V., Rives, S., Castellà, M., Alonso-Saladrigues, A., Benítez-Ribas, D., Caballero-Baños, M., Baumann, T., Cid, J., Garcia-Rey, E., Llanos, C., et al. (2021). CART19-BE-01: A Multicenter Trial of ARI-0001 Cell Therapy in Patients with CD19+ Relapsed/Refractory Malignancies. Mol. Ther. *29*, 636–644.
32. Ortiz-Maldonado, V., Rives, S., Espanol-Rego, M., Alonso-Saladrigues, A., Montoro, M., Magnano, L., Giné, E., Pascal, M., Díaz-Beyá, M., Castella, M., et al. (2021). Factors associated with the clinical outcome of patients with relapsed/refractory CD19(+) acute lymphoblastic leukemia treated with ARI-0001 CART19-cell therapy. J. Immunother. Cancer *9*, e003644.
33. Martínez-Cibrián, N., Ortiz-Maldonado, V., Español-Rego, M., Blázquez, A., Cid, J., Lozano, M., Magnano, L., Giné, E., Correa, J.G., Mozas, P., et al. (2024). The academic point-of-care anti-CD19 chimeric antigen receptor T-cell product varnimcabtagene autoleucel (ARI-0001 cells) shows efficacy and safety in the treatment of relapsed/refractory B-cell non-Hodgkin lymphoma. Br. J. Haematol. *204*, 525–533.
34. Frei, T., Cella, F., Tedeschi, F., Gutiérrez, J., Stan, G.B., Khammash, M., and Siciliano, V. (2020). Characterization and mitigation of gene expression burden in mammalian cells. Nat. Commun. *11*, 4641.
35. Hanson, G., and Coller, J. (2018). Codon optimality, bias and usage in translation and mRNA decay. Nat. Rev. Mol. Cell Biol. *19*, 20–30.
36. Hia, F., Yang, S.F., Shichino, Y., Yoshinaga, M., Murakawa, Y., Vandenbon, A., Fukao, A., Fujiwara, T., Landthaler, M., Natsume, T., et al. (2019). Codon bias confers stability to human mRNAs. EMBO Rep. *20*, e48220.
37. Schultz, L.M., Baggott, C., Prabhu, S., Pacenta, H.L., Phillips, C.L., Rossoff, J., Stefanski, H.E., Talano, J.A., Moskop, A., Margossian, S.P., et al. (2022). Disease Burden Affects Outcomes in Pediatric and Young Adult B-Cell Lymphoblastic Leukemia After Commercial Tisagenlecleucel: A Pediatric Real-World Chimeric Antigen Receptor Consortium Report. J. Clin. Oncol. *40*, 945–955.
38. Drent, E., Poels, R., Ruiter, R., van de Donk, N., Zweegman, S., Yuan, H., de Bruijn, J., Sadelain, M., Lokhorst, H.M., Groen, R.W., et al. (2019). Combined CD28 and 4-1BB Costimulation Potentiates Affinity-tuned Chimeric Antigen Receptor-engineered T Cells. Clin. Cancer Res. *25*, 4014–4025.
39. Zhao, Z., Condomines, M., van der Stegen, S.J.C., Perna, F., Kloss, C.C., Gunset, G., Plotkin, J., and Sadelain, M. (2015). Structural Design of Engineered Costimulation Determines Tumor Rejection Kinetics and Persistence of CAR T Cells. Cancer Cell *28*, 415–428.
40. Haso, W., Lee, D.W., Shah, N.N., Stetler-Stevenson, M., Yuan, C.M., Pastan, I.H., Dimitrov, D.S., Morgan, R.A., FitzGerald, D.J., Barrett, D.M., et al. (2013). Anti-CD22-chimeric antigen receptors targeting B-cell precursor acute lymphoblastic leukemia. Blood *121*, 1165–1174.
41. Fry, T.J., Shah, N.N., Orentas, R.J., Stetler-Stevenson, M., Yuan, C.M., Ramakrishna, S., Wolters, P., Martin, S., Delbrook, C., Yates, B., et al. (2018). CD22-targeted CAR T cells induce remission in B-ALL that is naive or resistant to CD19-targeted CAR immunotherapy. Nat. Med. *24*, 20–28.
42. Rufener, G.A., Press, O.W., Olsen, P., Lee, S.Y., Jensen, M.C., Gopal, A.K., Pender, B., Budde, L.E., Rossow, J.K., Green, D.J., et al. (2016). Preserved Activity of CD20-Specific Chimeric Antigen Receptor-Expressing T Cells in the Presence of Rituximab. Cancer Immunol. Res. *4*, 509–519.
43. Duell, J., Leipold, A.M., Appenzeller, S., Fuhr, V., Rauert-Wunderlich, H., Da Vià, M.C., Dietrich, O., Toussaint, C., Imdahl, F., Eisele, F., et al. (2023). Sequential Antigen-loss and Branching Evolution in Lymphoma after CD19- and CD20-Targeted T-cell Redirecting Therapy. Blood *143*, 685–696.
44. Foran, J.M., Norton, A.J., Micallef, I.N., Taussig, D.C., Amess, J.A., Rohatiner, A.Z., and Lister, T.A. (2001). Loss of CD20 expression following treatment with rituximab (chimaeric monoclonal anti-CD20): a retrospective cohort analysis. Br. J. Haematol. *114*, 881–883.
45. Grigg, S., Minson, A., Prins, E., and Dickinson, M.J. (2024). Relapse after glofitamab has a poor prognosis and rates of CD20 loss are high. Br. J. Haematol. *205*, 122–126.
46. Ereño-Orbea, J., Sicard, T., Cui, H., Mazhab-Jafari, M.T., Benlekbir, S., Guarné, A., Rubinstein, J.L., and Julien, J.P. (2017). Molecular basis of human CD22 function and therapeutic targeting. Nat. Commun. *8*, 764.
47. Kokalaki, E., Ma, B., Ferrari, M., Grothier, T., Hazelton, W., Manzoor, S., Costu, E., Taylor, J., Bulek, A., Srivastava, S., et al. (2023). Dual targeting of CD19 and CD22 against B-ALL using a novel high-sensitivity aCD22 CAR. Mol. Ther. *31*, 2089–2104.
48. Friedman, K.M., Garrett, T.E., Evans, J.W., Horton, H.M., Latimer, H.J., Seidel, S.L., Horvath, C.J., and Morgan, R.A. (2018). Effective Targeting of Multiple B-Cell Maturation Antigen-Expressing Hematological Malignances by Anti-B-Cell Maturation Antigen Chimeric Antigen Receptor T Cells. Hum. Gene Ther. *29*, 585–601.
49. Oliver-Caldes, A., Español-Rego, M., Zabaleta, A., González-Calle, V., Navarro-Velázquez, S., Inogés, S., de Cerio, A.L.D., Cabañas, V., López-Muñoz, N., Rodríguez-Otero, P., et al. (2024). Biomarkers of Efficacy and Safety of the Academic BCMA-CART ARI0002h for the Treatment of Refractory Multiple Myeloma. Clin. Cancer Res. *30*, 2085–2096.
50. Ruella, M., Barrett, D.M., Kenderian, S.S., Shestova, O., Hofmann, T.J., Perazzelli, J., Klichinsky, M., Aikawa, V., Nazimuddin, F., Kozlowski, M., et al. (2016). Dual CD19 and CD123 targeting prevents antigen-loss relapses after CD19-directed immunotherapies. J. Clin. Invest. *126*, 3814–3826.
51. Fernandez de Larrea, C., Staehr, M., Lopez, A.V., Ng, K.Y., Chen, Y., Godfrey, W.D., Purdon, T.J., Ponomarev, V., Wendel, H.G., Brentjens, R.J., et al. (2020). Defining an Optimal Dual-Targeted CAR T-cell Therapy Approach Simultaneously Targeting BCMA and GPRC5D to Prevent BCMA Escape-Driven Relapse in Multiple Myeloma. Blood Cancer Discov. *1*, 146–154.
52. Olivera, I., Bolaños, E., Gonzalez-Gomariz, J., Hervas-Stubbs, S., Mariño, K.V., Luri-Rey, C., Etxeberria, I., Cirella, A., Egea, J., Glez-Vaz, J., et al. (2023). mRNAs encoding IL-12 and a decoy-resistant variant of IL-18 synergize to engineer T cells for efficacious intratumoral adoptive immunotherapy. Cell Rep. Med. *4*, 100978.
53. Ghorashian, S., Lucchini, G., Richardson, R., Nguyen, K., Terris, C., Guvenel, A., Oporto-Espuelas, M., Yeung, J., Pinner, D., Chu, J., et al. (2024). CD19/CD22 targeting with cotransduced CAR T cells to prevent antigen-negative relapse after CAR T-cell therapy for B-cell ALL. Blood *143*, 118–123.
54. Juan, M., Delgado, J., Calvo, G., Trias, E., and Urbano-Ispizua, Á. (2021). Is Hospital Exemption an Alternative or a Bridge to European Medicines Agency for Developing Academic Chimeric Antigen Receptor T-Cell in Europe? Our Experience with ARI-0001. Hum. Gene Ther. *32*, 1004–1007.
55. Calderon, H., Mamonkin, M., and Guedan, S. (2020). Analysis of CAR-Mediated Tonic Signaling. In Chimeric Antigen Receptor T Cells: Development and Production, K. Swiech, K.C.R. Malmegrim, and V. Picanço-Castro, eds. (Springer US), pp. 223–236.
56. Andreu-Saumell, I., Rodriguez-Garcia, A., Mühlgrabner, V., Gimenez-Alejandre, M., Marzal, B., Castellsagué, J., Brasó-Maristany, F., Calderon, H., Angelats, L., Colell, S., et al. (2024). CAR affinity modulates the sensitivity of CAR-T cells to PD-1/PD-L1-mediated inhibition. Nat. Commun. *15*, 3552.
57. Guedan, S., Chen, X., Madar, A., Carpenito, C., McGettigan, S.E., Frigault, M.J., Lee, J., Posey, A.D., Jr., Scholler, J., Scholler, N., et al. (2014). ICOS-based chimeric antigen receptors program bipolar TH17/TH1 cells. Blood *124*, 1070–1080.
58. Abramson, J., Adler, J., Dunger, J., Evans, R., Green, T., Pritzel, A., Ronneberger, O., Willmore, L., Ballard, A.J., Bambrick, J., et al. (2024). Accurate structure prediction of biomolecular interactions with AlphaFold 3. Nature *630*, 493–500.
59. Dobano-Lopez, C., Valero, J.G., Araujo-Ayala, F., Nadeu, F., Gava, F., Faria, C., Norlund, M., Morin, R., Bernes-Lasserre, P., Arenas, F., et al. (2024). Patient-derived follicular lymphoma spheroids recapitulate lymph node signaling and immune profile uncovering galectin-9 as a novel immunotherapeutic target. Blood Cancer J. *14*, 75.

**YMTHE, Volume *33***

## Supplemental Information

# ARI0003: Co-transduced CD19/BCMA dual-targeting CAR-T cells for the treatment of non-Hodgkin lymphoma

**Mireia Bachiller, Nina Barceló-Genestar, Alba Rodriguez-Garcia, Leticia Alserawan, Cèlia Dobaño-López, Marta Giménez-Alejandre, Joan Castellsagué, Salut Colell, Marc Otero-Mateo, Asier Antoñana-Vildosola, Marta Español-Rego, Noelia Ferruz, Mariona Pascal, Beatriz Martín-Antonio, Xavier M. Anguela, Cristina Fillat, Eulàlia Olesti, Gonzalo Calvo, Manel Juan, Julio Delgado, Patricia Pérez-Galán, Álvaro Urbano-Ispizua, and Sonia Guedan**

# Supplemental Figures

## Figure S1

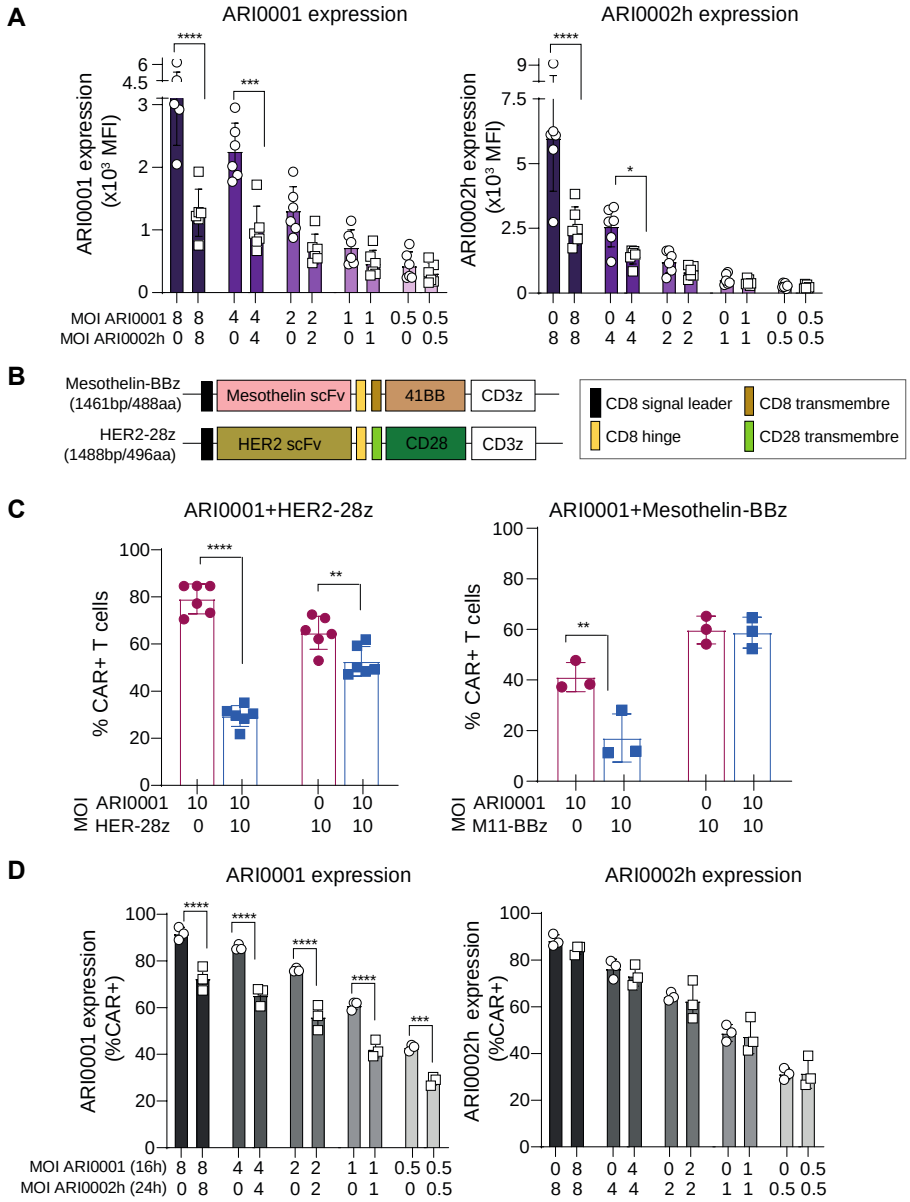


**Figure S1. Characterization of ARI0001 and ARI0002h co-transduction.** T cells were activated using CD3/CD28 beads and 24 hours later (unless otherwise indicated) transduced with the indicated MOI of the different lentiviral vectors (as single vectors or in co-transduction). Analysis of CAR expression was performed at day 6 of CAR-T cell expansion using recombinant proteins in a minimum of three different healthy donors. Each dot/square represents an individual donor. **A)** Co-transduction of lentiviral vectors expressing ARI0001 or ARI0002h at equivalent MOIs resulted in decreased mean fluorescent intensity (MFI) for both CARs compared to single transductions. **B)** Schematic representation of CAR constructs, showing base pair lengths and amino acid

sequences. Both CARs feature the CD8α signal peptide and extracellular spacer. Mesothelin-BBz incorporates the CD8α transmembrane domain with the 4-1BB co-stimulatory domain, while HER2-28z includes the CD28 transmembrane domain with CD28 co-stimulatory domain. **C)** Percentage of CAR expression on the T cell membrane in single compared to co-transduced CAR-T cells, assessed by flow cytometry (n=3-6 healthy donors). **D)** Transduction of T cells with ARI0002h-expressing lentiviral vectors 8 hours after the addition of ARI0001. ARI0001 expression is shown in the left panel and ARI0002h in the right panel. Statistical significance in A-D was determined using two-way ANOVA. *P*-values: ****<0.0001, ***<0.0005, **<0.005, *<0.05.

## Figure S2

A

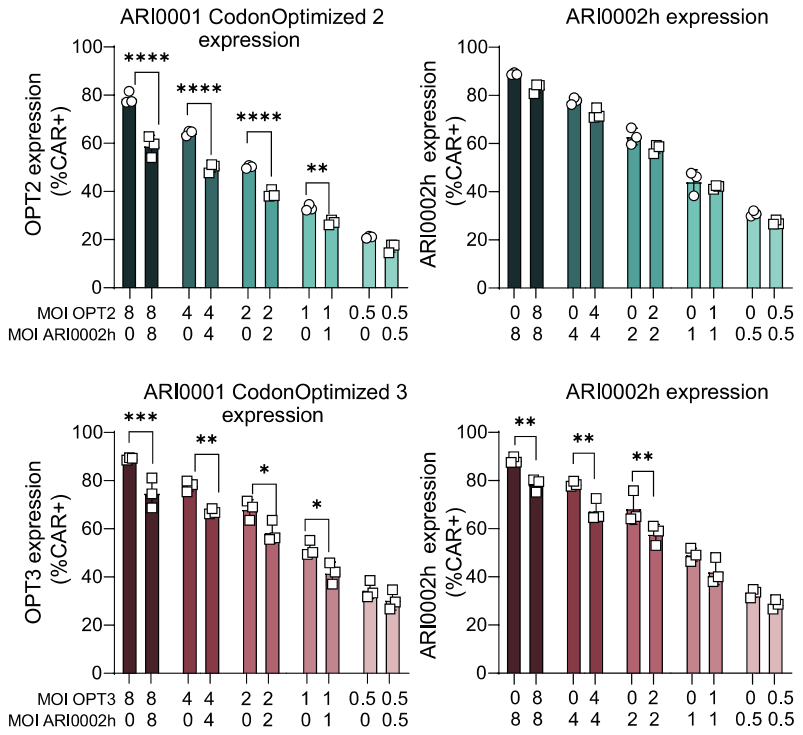


B

| Name | Length | CAI | %GC | %GC1 | %GC2 | %GC3 |
|---|---|---|---|---|---|---|
| ARI0001 (no CodonOptimized) | 1509 | 0.852 | 56.7 | 59.4 | 50.9 | 59.8 |
| ARI0001 CodonOptimized 1 | 1509 | 0.810 | 61.6 | 59.8 | 51.1 | 73.8 |
| ARI0001 CodonOptimized 2 | 1509 | 0.812 | 61.6 | 60.2 | 51.1 | 73.6 |
| ARI0001 CodonOptimized 3 | 1509 | 0.816 | 61.3 | 59.8 | 51.1 | 73.0 |

C

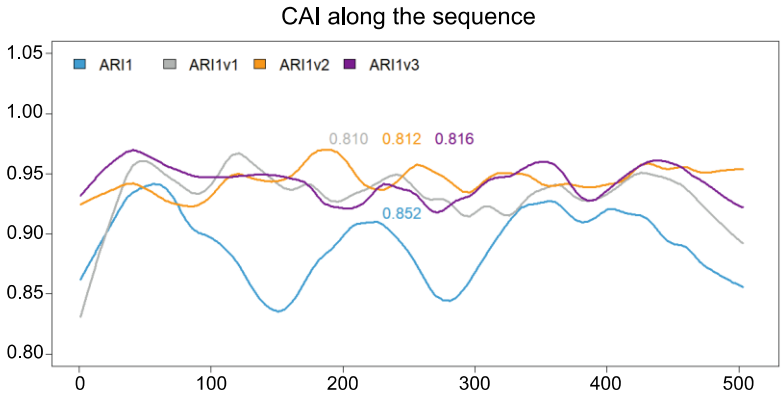


D

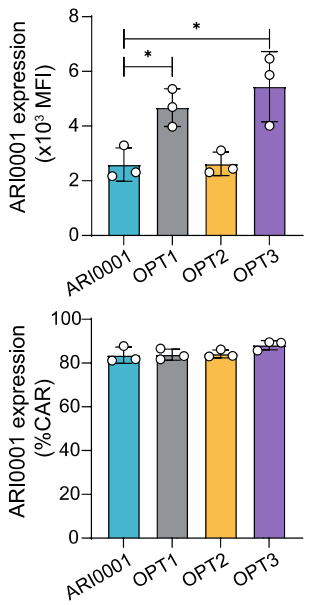

**Figure S2. ARI0001 codon optimization did not improve its expression in co-transduction with ARI0002h**. **A)** T cells were activated with CD3/CD28 beads and 24 hours later transduced with the indicated MOI of the different lentiviral vectors (as single vectors or in co-transduction). Analysis of CAR expression was performed at day 6 of CAR-T cell expansion using recombinant proteins (CD19-Fc and BCMA-His) followed by a secondary antibody (against Fc or His) in a minimum of three different healthy donors. When co-transducing two lentiviral vectors, one or both CARs were expressed at lower levels on the T cell membrane than when transduced individually. Impaired CAR expression in dual CAR-T cells was exacerbated when increasing multiplicities of infection (MOI) were used. Co-transduction of codon-optimized versions of ARI0001 with ARI0002h did not improve ARI0001 expression in co-transduction. **B)** Table of codon usage analysis of CD19 sequences corresponding to ARI0001 versions. Global CAI, average GC content and the % of GC at positions 1, 2 and 3 of the different codons are indicated. **C)** Representation of the CAI along the non-optimized and optimized DNA sequences encoding CD19 protein from the different ARI0001 versions. **D)** Quantification of CAR expression presented in the upper panel as MFI and in the lower panel as the percentage of expression for ARI0001 and its codon-optimized versions in single transductions. Statistical analyses were performed using Two-way ANOVA tests, with p-values denoted as ****<0.0001, ***<0.0005, **<0.005, *<0.05. The data represents the Mean ± SD from n=3 healthy donors.

**Figure S3**

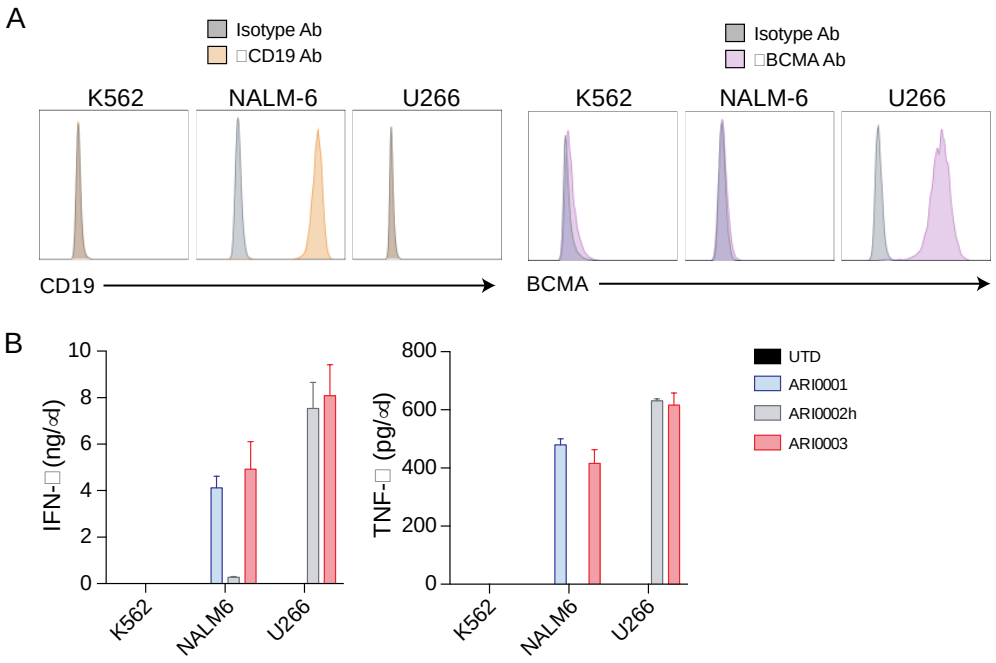


**Figure S3. ARI0003 activation in the absence of target antigens or in the presence of a single target antigen. A)** Analysis of the expression of CD19 and BCMA in control cell lines K562 ($CD19^{-}BCMA^{-}$), NALM-6 ($CD19^{+}BCMA^{-}$) and U266 ($CD19^{-}BCMA^{+}$) by flow cytometry. **B)** Monospecific CAR-T cells (ARI0001 and ARI0002h) and dual CAR-T cells (ARI0003) were cultured with the indicated target cells at an E:T=3:1. IFN-γ and TNF-α cytokine release in supernatants was analyzed by ELISA 24h after co-culture. The mean ± SD of triplicates from a healthy donor is shown. These experiments have been repeated twice, with two different healthy donors, with similar results.

## Figure S4

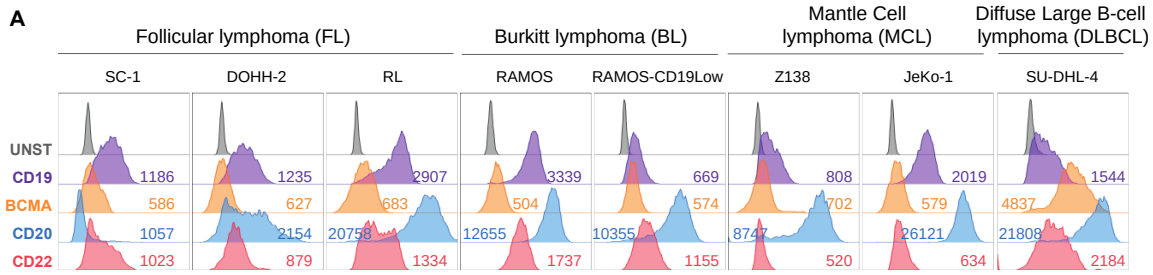


**Figure S4. Expression of CD19, BCMA, CD20 and CD22 in a panel of non-Hodgkin's lymphoma tumor lines. A)** Antigen expression was analyzed by flow cytometry. The panel includes cell lines from follicular lymphoma (SC-1, DOHH-2 and RL), Burkitt lymphoma (Ramos WT and Ramos CD19 Low), mantle cell lymphoma (Z138 and JeKo-1) and diffuse large B-cell lymphoma (SU-DHL-4).

## Figure S5

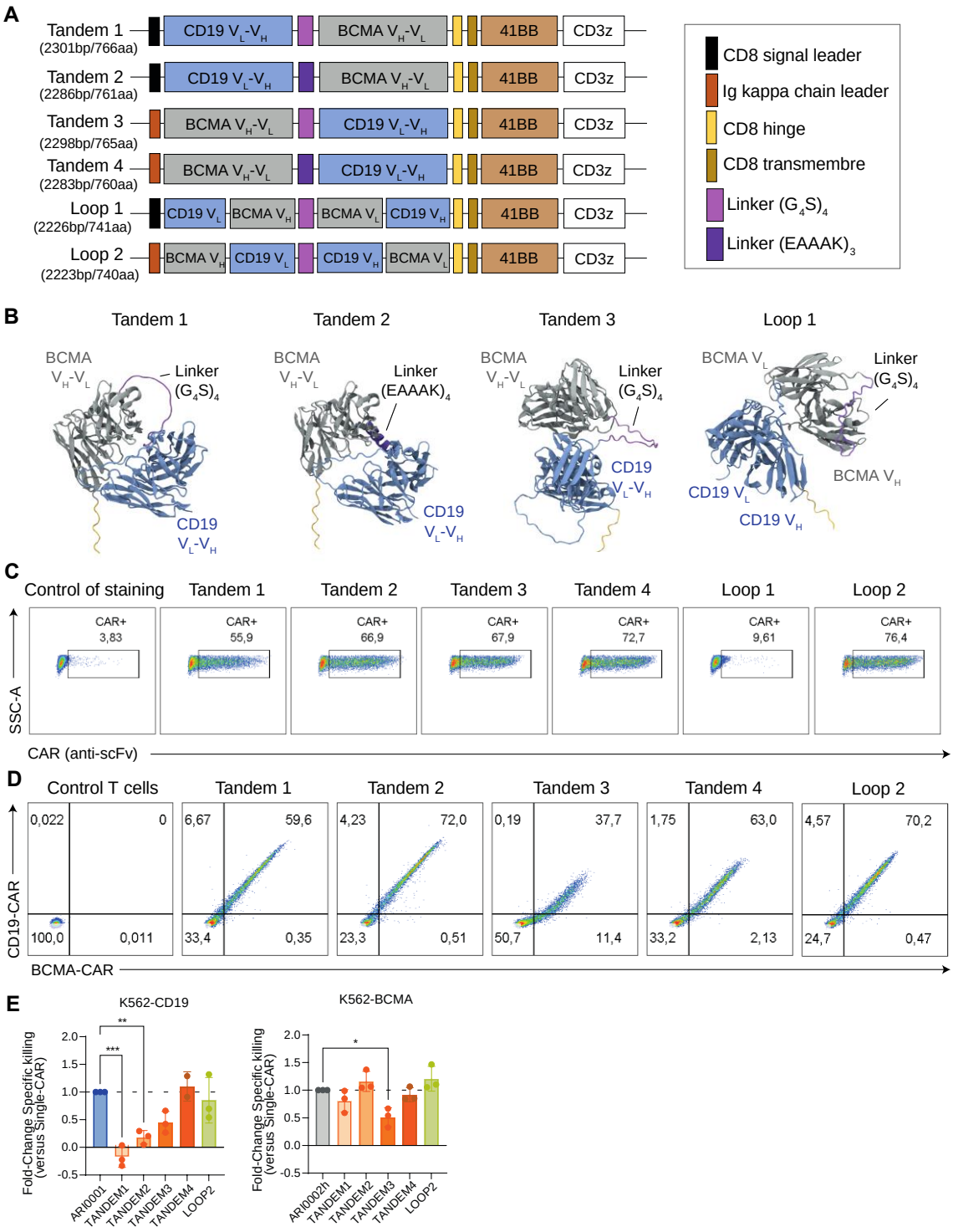


**Figure S5. Selection of tandem and loop constructs based on CAR surface expression and specific lysis against targeted antigens. A)** Schematic representation of the different tandem and loop CAR constructs. **B)** Structural models of the Tandem (Tandem1-3) and Loop (Loop1-2) constructs were generated using AlphaFold3. The models were based on the input sequences of their extracellular domains, specifically the CD8a hinge and scFv. The BCMA-targeting regions are

represented in grey, the CD19-targeting regions in blue, and the linkers connecting both regions are shown in purple. Structure of single CARs, ARI0001 and ARI0002h and selected Tandem4 and Loop2 are shown in Figure 3B. **C-D)** Representative flow cytometry plots displaying CAR expression on T Cells using anti-mouse IgG antibody (C) or recombinant proteins (D). **E)** Indicated CAR-T cells and target cells were mixed at an E:T=1:1 and cytotoxicity was evaluated 24 hours later in a luciferase-based assay. All data are means ± SD from triplicate wells of a representative healthy donor. Dotted lines indicate the percentage of lysis of ARI0001 in the K562-CD19 cell line and ARI0002h in the K562-BCMA cell line. Fold-change in specific lysis for each CAR-T cell group is shown in n=3 healthy donors.

**Figure S6**

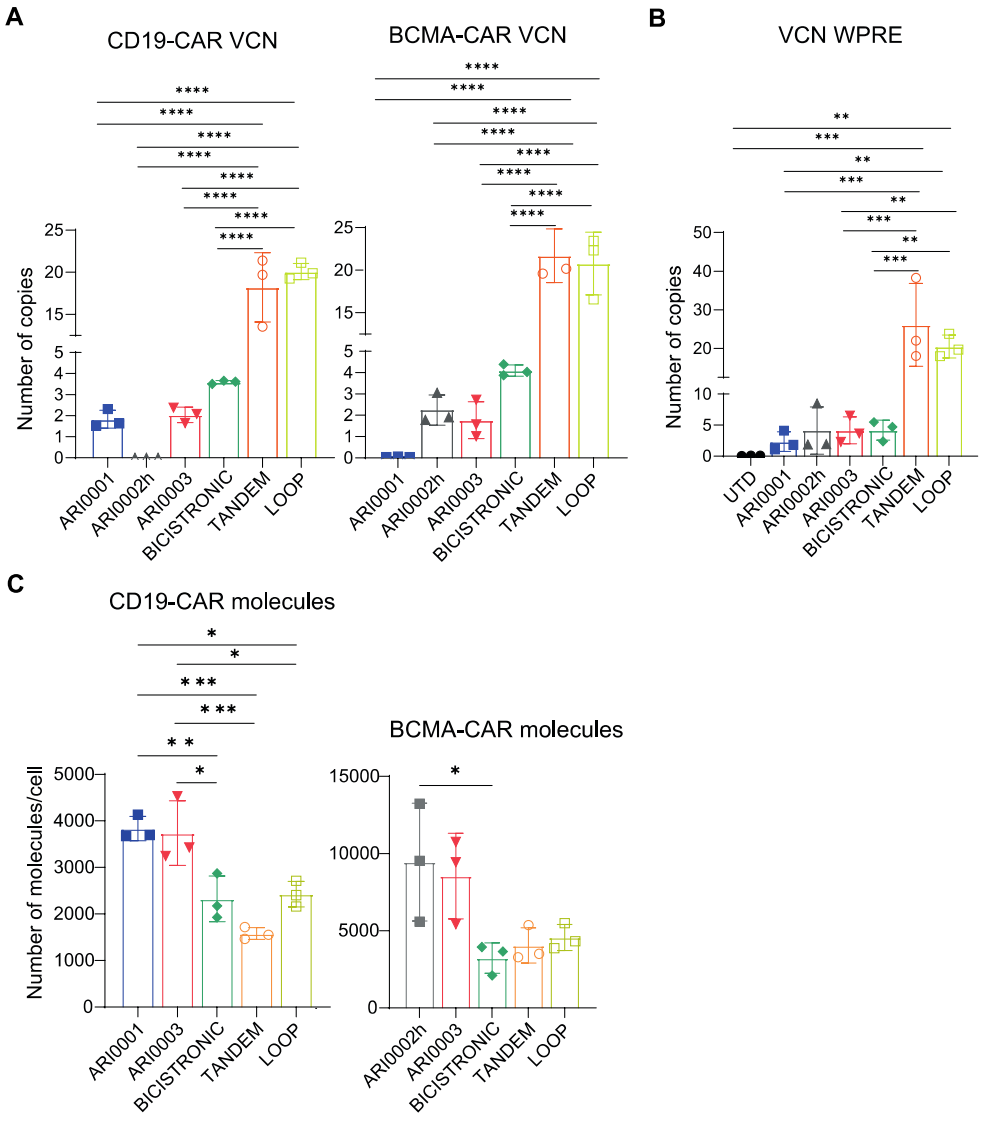


**Figure S6. Expression profile of various dual CAR-T Cell Modalities. A-B)** Single and dual-targeting strategies were studied at the level of DNA. The absolute number of lentiviral DNA copies integrated per genome for CD19-CARs and BCMA-CARs was assessed using qPCR using specific primers for CD19 scFv and BCMA scFv (A) or using specific primers targeting WPRE (B). Each dot is a healthy donor (n=3). Statistical significance was assessed using a one-way ANOVA test, with p-values defined as follows: ****<0.0001, ***<0.0005, **<0.005. **C)** The absolute number of CAR molecules for both single and dual-targeting strategies was evaluated using Quantibrite technology. Each dot represents a healthy donor (n=3). Statistical significance was determined through a one-way ANOVA test, with p-values indicated as: ****<0.0001, ***<0.0005, **<0.005, *<0.05.

**Figure S7**

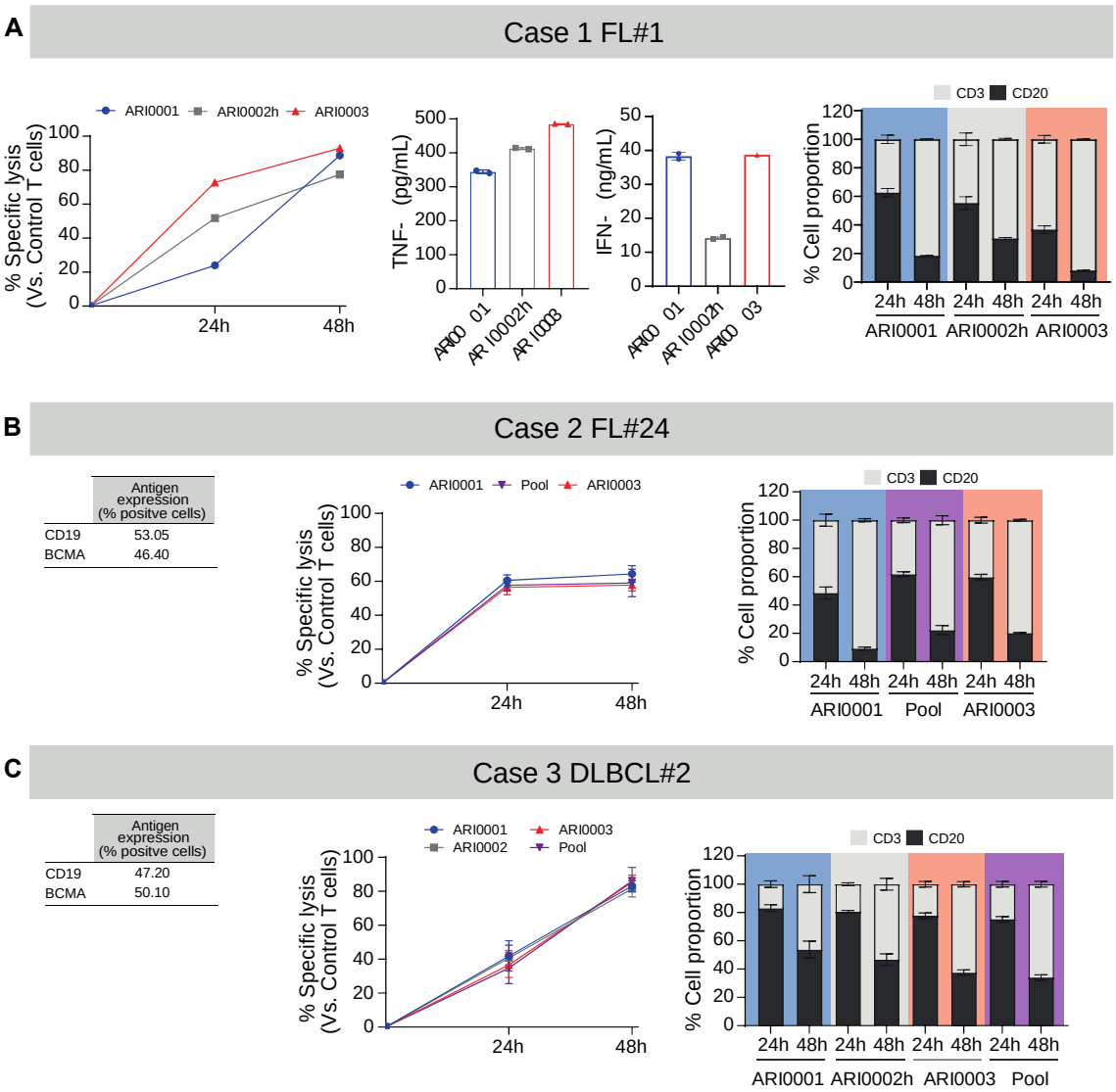


**Figure S7. PDLS as pre-clinical model for CAR-T cells.** Patient derived NHL spheroids (PDSL) from FL (A, B) and DLBCL (C) were generated. Specific lysis of remaining tumor cells was analyzed by flow cytometry after co-culture at E:T=1:2 ratio at indicated time-points. Cytokine production by ELISA (TNF-α and IFN-γ) after 24h co-culture at E:T=1:2 was assessed. Each dot in the ELISA represents a spheroid (n=1-2). CD19 and BCMA antigen expression was analyzed before CAR-T cell addition for co-culture. Percentage cell proportion was analyzed after 24h and 48h co-culture by flow cytometry. Results represent the mean ± SD for triplicates.

**Figure S8**

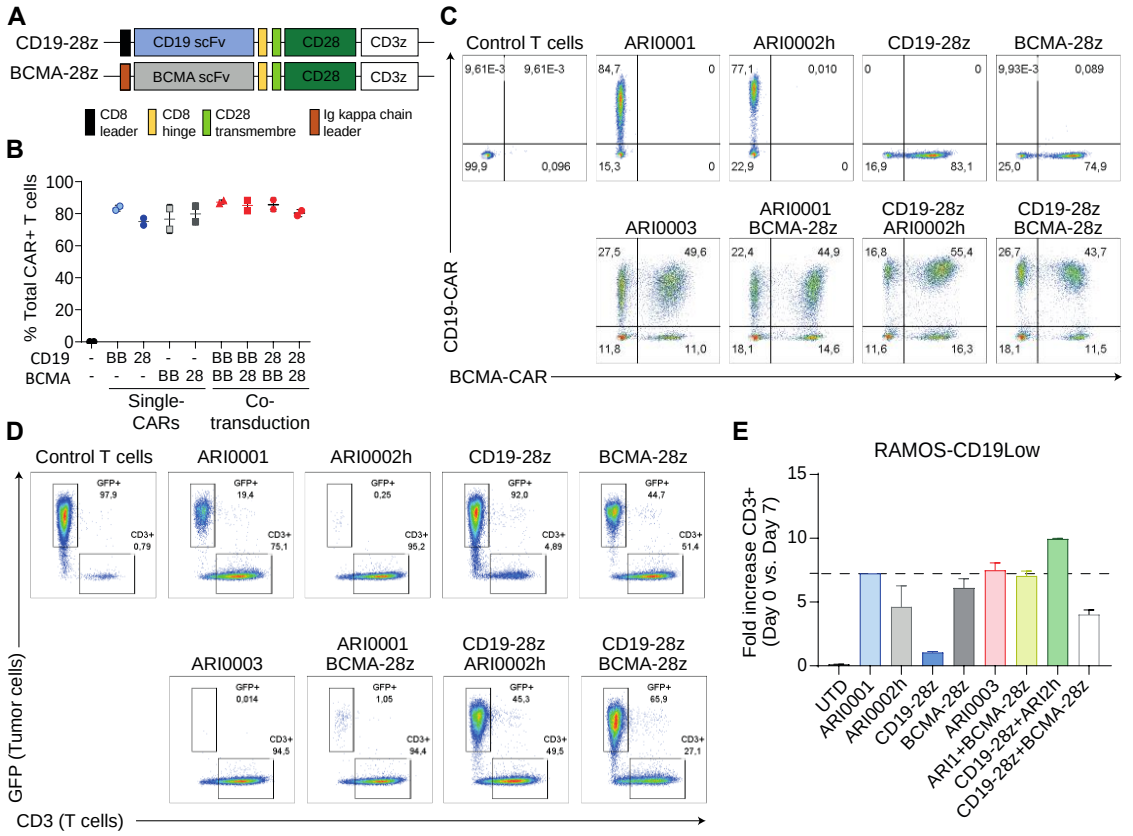


**Figure S8. Generation and evaluation of dual CAR-T cells containing different intracellular domains. A)** Schematic representation of CD28-based CAR constructs. **B)** Percentage of T cells expressing CARs at the cell surface as analyzed by flow cytometry. Each dot represents a healthy donor (n=2). **C)** Flow cytometry plots illustrating CD19-CAR and/or BCMA-CAR expression on the T cell membrane. **D-E)** Long-term cytotoxicity and proliferation of dual CAR-T cells in co-culture with Ramos –CD19 Low. The different groups of single- and co-transduced CAR-T cells or untransduced control T cells (UTD) were co-cultured with Burkitt lymphoma cells modified to express low levels of CD19 (Ramos –CD19 Low) at E:T=1:4. 7 days after co-culture, cells were harvested and stained with specific antibodies to be analyzed by flow cytometry. Cells were selected for live/dead, CD3 (for T cells) or GFP (for tumor cells). **D)** CD3+ (T lymphocytes) and GFP+ (tumor) populations after 7 days of co-culture. **E)** The proliferation of T lymphocytes after 7 days of co-culture with target cells was analyzed by flow cytometry using quantification beads. Dotted line indicates ARI0001 proliferation. All data are means ± SD from duplicate wells of a healthy donor.

**Figure S9**

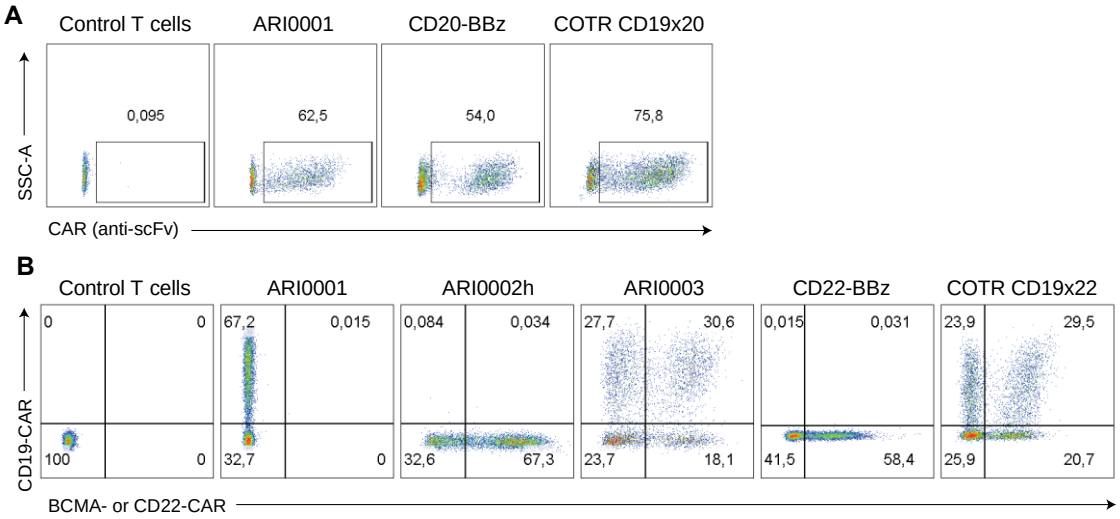


**Figure S9. CAR expression frequencies in transduced T cell populations.** CAR expression on the T cell membrane was analyzed by flow cytometry using (A) anti-mouse IgG antibody for CD20-CAR or (B) recombinant proteins for CD22-CAR. Flow plots are representative of one healthy donor.

## Figure S10

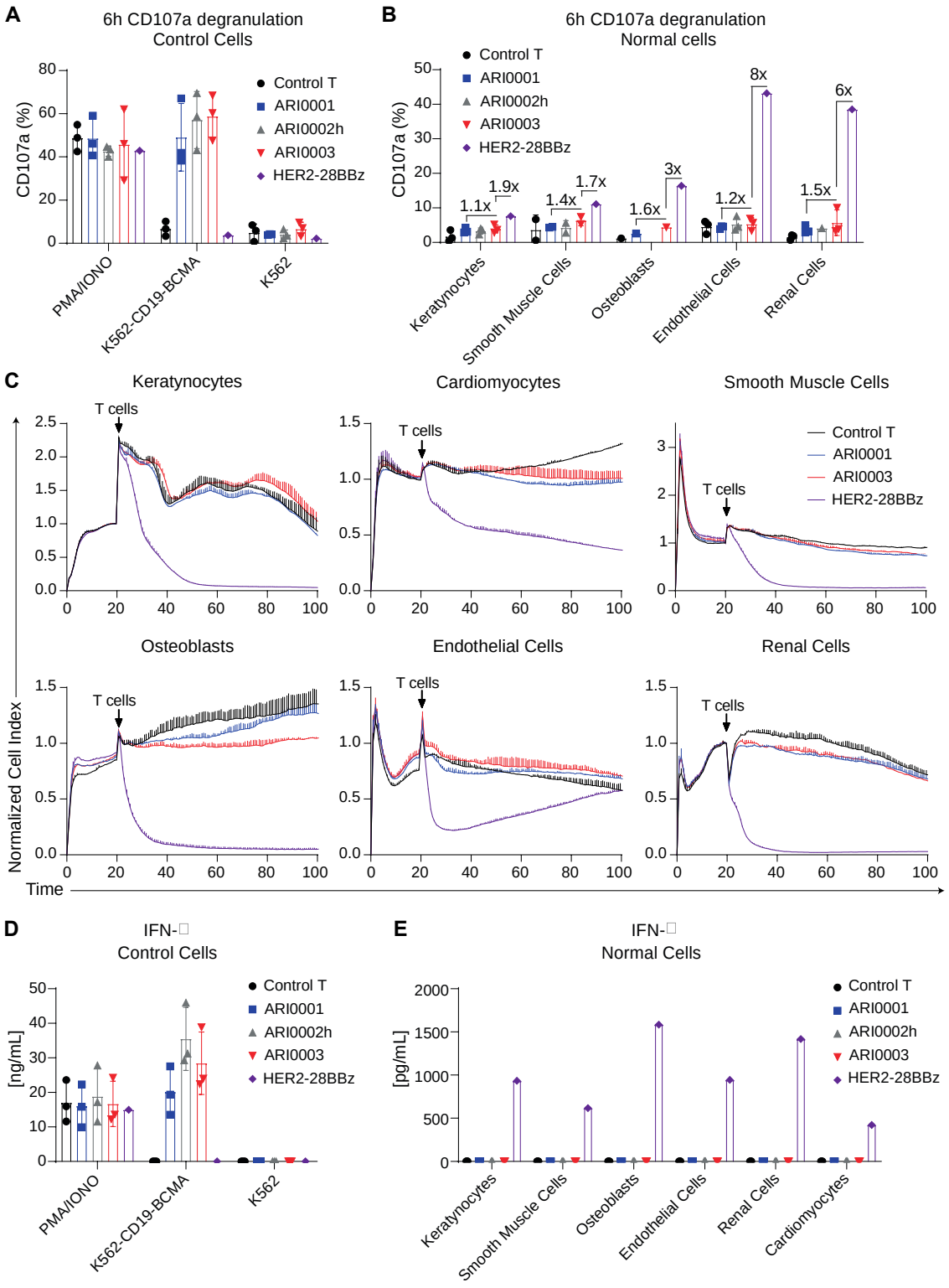
A
6h CD107a degranulation
Control Cells
CD107a (%)
Control T
ARI0001
ARI0002h
ARI0003
HER2-28BBz
PMA/IONO
K562-CD19-BCMA
K562
B
6h CD107a degranulation
Normal cells
1.1x
1.9x
1.4x
1.7x
1.6x
3x
1.2x
8x
1.5x
6x
Keratynocytes
Smooth Muscle Cells
Osteoblasts
Endothelial Cells
Renal Cells
C
Keratynocytes
Cardiomyocytes
Smooth Muscle Cells
Osteoblasts
Endothelial Cells
Renal Cells
T cells
Normalized Cell Index
Time
D
IFN-γ
Control Cells
[ng/mL]
E
IFN-γ
Normal Cells
[pg/mL]

**Figure S10. Dual CD19/BCMA targeting by ARI0003 cells does not induce degranulation, killing and cytokine production when co-cultured with normal cells. A-B)** Indicated CAR-T cells were stimulated with stimulation cocktail (PMA/ionomycin), co-cultured with K562-CD19-BCMA or K562 tumor cells or normal cells at an E:T=1:1. The percentage of T cells expressing CD107a was analyzed by flow cytometry 6 hours after co-culture. The fold-change in CD107a expression in ARI0003 CAR-T cells versus ARI0001 or high affinity HER2-28BBz CAR-T cells is shown for each cell line. **C)** A real-time cytotoxicity assay (xCelligence) was used to evaluate the lysis of normal cells when treated with control T cells or CAR-T cells at an E:T=3:1 over a 100-hour period. **D)** Indicated CAR-T cells were stimulated with stimulation cocktail or co-cultured with K562-CD19-BCMA (positive control), K562 (negative control) and normal cells at an E:T=3:1. Supernatants were obtained 24 hours after co-culture and IFN-γ production was analyzed by ELISA. Each dot represents a healthy donor.

**Table S1. FL patients characteristics.**

[1]F: Female, M: Male; [2] PB: Peripheral Blood, LN: Lymph Node, BM: Bone marrow. [3] Samples were obtained at D: diagnosis, R: relapse, Pt: Pretreatment, NA: Not Available; [4]Evaluated by two independent pathologists; [5]Ann Arbor stage; [6]FLIPI: Follicular Lymphoma International Prognostic Index (High (H):≧3; Medium (M):2; Low (L):0-1); [7]All treatments; R: Rituximab; R-mnt: Maintenance Rituximab; RTx: Radiotherapy; GA: Obinutuzumab; Benda: Bendamustine; CHOP: Chemotherapy combination of Cyclophosphamide Hydroxydaunorubicin, Oncovin and Prednisone; ASCT: Autologous Stem Cell Transplantation;DA-EPOCH: dose adjusted combination of etoposide phosphate, prednisone, vincristine sulfate (Oncovin), cyclophosphamide, and hydroxydaunorubicin; ICE: ifosfamide, carboplatin, and etoposide; GEMOX: gemcitabine-oxaliplatin: IT therapy: inthratecal therapy. CR: Complete Response; PR: Partial Response; SD: Stable Disease; [9]POD24: Progression of disease within 2 years; [10] from B-cell panel (CD19, C20, CD22 and CD79b) in routine diagnosis. Y: Yes; N: No; N/A: Not available.

| **Study label** | **Sex /Age[1]** | **Sample type[2]** | **Disease status at sampling[3]** | **Histological grade[4]** | **Stage[5]** | **FLIPI6** | **Treatments[7]** | **Response to 1st tt[8]** | **POD24[9]** | **Cell count Lympho B ($10^9$/L)** | **% Lympho B[10]** |
|---|---|---|---|---|---|---|---|---|---|---|---|
| FL1 | F/75 | PB | D | 2 | IVA | H | R-COP/R-mnt | PR | N | 74.46 | 78 |
| FL2 | F/52 | LN | D | 1 | IV | H | R-CHOP/P-mnt<br>R-ESHAP<br>ASCT<br>R-GEMOX<br>Ifosfamide<br>Rx<br>CD19 CART (axi-cel) | CR | N | 3.13 | 85 |
| FL24 | F/51 | PB | D | 2 | IV | H | R-CHOP/P-mnt | CR | N | 9.64 | 70 |

**Table S2. DLBCL patients characteristics.**

[1]F: Female, M: Male; [2] PB: Peripheral Blood, LN: Lymph Node, BM: Bone marrow. [3] Samples were obtained at D: diagnosis, R: relapse, Pt: Pretreatment, NA: Not Available; [4]Evaluated by two independent pathologists; [5]Ann Arbor stage; [6]FLIPI: Follicular Lymphoma International Prognostic Index (High (H):≧3; Medium (M):2; Low (L):0-1); [7]All treatments; R: Rituximab; R-mnt: Maintenance Rituximab; RTx: Radiotherapy; GA: Obinutuzumab; Benda: Bendamustine; CHOP: Chemotherapy combination of Cyclophosphamide Hydroxydaunorubicin, Oncovin and Prednisone; ASCT: Autologous Stem Cell Transplantation;DA-EPOCH: dose adjusted combination of etoposide phosphate, prednisone, vincristine sulfate (Oncovin), cyclophosphamide, and hydroxydaunorubicin; ICE: ifosfamide, carboplatin, and etoposide; GEMOX: gemcitabine-oxaliplatin: IT therapy: inthratecal therapy. CR: Complete Response; PR: Partial Response; SD: Stable Disease; [9]POD24: Progression of disease within 2 years; [10] from B-cell panel(CD19, C20, CD22 and CD79b) in routine diagnosis. Y: Yes; N: No; N/A: Not available. *progression after CD19 CAR-T therapy

| **Study label** | **Sex /Age[1]** | **Sample type[2]** | **Disease status at sampling[3]** | **Subtype** | **Stage[5]** | **Genetic alterations** | **Treatments[7]** | **Response to 1st tt[8]** |
|---|---|---|---|---|---|---|---|---|
| DLBCL2 | M/37 | LN | D | DLBCL | IE | del1p36, BCL6 gains | R-CHOP +RTx | CR |
| DLBCL4 | M/54 | PB | R* | GC-DLBCL (from tFL) | IVB | N/A | RTx +R-DA-EPOCH+IT therapy<br>RTx<br>ASCT<br>R-ICE<br>R-GEMOX<br>CD19 CART (aci-cel) | PR |
| DLBCL5 | M/30 | BM | R* | HGBCL, NOS | IVB | delTP53, t(8;14)(q24;q32) | BURKIMAB-14<br>R-HyperCVAD<br>CD19 CART (ARI0001) | CR |

# Supplemental Methods

## Codon usage analysis

Homo sapiens codon usage was extracted from the Codon Usage Database available at http://www.kazusa.or.jp/codon/. Codon Adaptation Index (CAI) along the sequence was represented using R v3.2.3 software. The Codon Adaptation Index (CAI) of each sequence, the percentage of GC and the percentage of codons with G or C at the first %GC1, second %GC2 or third position %GC3 were calculated using the CAIcal server from http://ppuigbo.me/programs/CAIcal/[19].